Journal of the Geological Society, London, Vol. **166**, 2009, pp. 431–445. doi: 10.1144/0016-76492007-177.

Palaeoenvironmental significance of carbon- and oxygen-isotope stratigraphy of marine Triassic–Jurassic boundary sections in SW Britain

CHRISTOPH KORTE[1]*, STEPHEN P. HESSELBO[1], HUGH C. JENKYNS[1], ROSALIND E. M. RICKABY[1] & CHRISTOPH SPÖTL[2]

[1]*Department of Earth Sciences, University of Oxford, Parks Road, Oxford OX1 3PR, UK*

[2]*Institut für Geologie und Paläontologie, Universität Innsbruck, Innrain 52, A-6020 Innsbruck, Austria*

**Corresponding author (e-mail: korte@geo.ku.dk)*

Abstract: Carbon-isotope stratigraphy is a useful tool for stratigraphic correlation, especially for strata deposited during major perturbations of the carbon cycle that affected the marine, terrestrial and atmospheric reservoirs. For the Triassic–Jurassic boundary, effectively defined by a first-order mass extinction, major fluctuations in carbon-isotope values have been well documented, but these datasets have generally been derived from bulk-rock samples. Hence, the extent to which features of the isotopic curve reflect diagenetic alteration or changing proportions of constituent materials is unconstrained. Here, carbon- and oxygen-isotope data are presented from well-preserved oyster shells (*Liostrea*) comprising low-magnesium calcite, a mineral species relatively resistant to diagenetic alteration. Samples were obtained from Lavernock Point, Glamorgan, Wales, a coastal section close to a candidate stratotype for the base of the Jurassic at St Audrie's Bay, Somerset, England. The carbon-isotope signature from St Audrie's Bay, previously defined on the basis of analysis of bulk organic matter, is confirmed by our new data. Major features are (1) the upper part of an 'initial' negative isotope excursion in the lowest part of the section, followed by (2) a pronounced positive excursion, and (3) an extended 'main' negative isotope excursion in the highest part of the section. The data confirm that the carbon-isotope stratigraphy previously documented from bulk organic matter in SW England records the chemical composition of the contemporaneous seawater. Bulk carbonates sampled over the same interval near Lyme Regis, England, show similar trends to those from oyster calcite in the lower part of the study section, but there are more ^{13}C-depleted values up-section. These lower values probably result from an admixture of primary and diagenetic carbonate. Palaeotemperatures calculated from oxygen-isotope values from Lavernock Point oyster shells are relatively cool at the beginning of the positive carbon-isotope excursion, and increased by up to 10 °C during the main negative carbon-isotope excursion. The new results are compatible with the view that positive carbon-isotope excursions correspond to times of low atmospheric carbon dioxide content, whereas negative carbon-isotope excursions correspond to times of high atmospheric carbon dioxide content, as is also found to be the case during the Early Jurassic (Toarcian) Oceanic Anoxic Event. The Mg/Ca and Sr/Ca ratios and $\delta^{18}O$ of investigated *Liostrea hisingeri* show no correlation, supporting data from modern bivalves that indicate that incorporation of Mg and Sr is controlled mainly by factors other than temperature.

The Triassic–Jurassic (T–J) transition, *c*. 200 Ma ago, was a time of mass extinction that affected both the marine and continental biota (Hallam & Wignall 1997, and references therein). The patterns of environmental change that accompanied the extinction, and the cause or causes, are vigorously debated (see, e.g. Hesselbo *et al*. 2007*a*, for summary). As is the case for many other episodes of major environmental change, the T–J boundary is characterized by major perturbations to the carbon cycle, demonstrated by carbon-isotope profiles generated from several parts of the world (McRoberts *et al*. 1997; Pálfy *et al*. 2001, 2007; Ward *et al*. 2001, 2007; Hesselbo *et al*. 2002, 2004; Guex *et al*. 2004; Galli *et al*. 2005, 2007; Kuerschner *et al*. 2007; Williford *et al*. 2007). Although there is generally good agreement between the shapes of curves from different regions, a shortcoming of the carbon-isotope profiles published hitherto is that they are almost entirely based on analyses of bulk organic matter or bulk carbonate, where the exact nature, origin and proportion of the components is indeterminate. The few existing data from diagenetically unaltered marine skeletal low-Mg calcite are not sufficient to construct stratigraphically extended isotope curves (e.g. van de Schootbrugge *et al*. 2007). Here, analyses of shell material from the oyster *Liostrea hisingeri* (Nilsson) are presented, carefully screened for diagenetic alteration, and collected from numerous horizons across and above the T–J boundary in SW Britain.

Similarities between the T–J boundary events and those occurring during Phanerozoic Oceanic Anoxic Events have been highlighted by a number of workers (e.g. Cohen & Coe 2002; Jenkyns *et al*. 2002). Apart from the development of large-amplitude carbon-isotope excursions, similarities include anomalies and trend reversals in Sr and Os isotope records (Korte *et al*. 2003; Cohen & Coe 2007), and rapid turnover or crises amongst shallow-marine carbonate-producing organisms (Hautmann 2006; Kiessling *et al*. 2007; Tomašových & Siblík 2007). It has been shown for other intervals of major environmental change that carbon-isotope fluctuations are correlated with marine and atmospheric palaeotemperature fluctuations, and such co-variations have to be taken into account during consideration of the forcing functions involved (e.g. Jenkyns 2003). Although data for palaeotemperature changes accompanying T–J boundary events are debated (e.g. McElwain *et al*. 1999; Hubbard & Boulter 2000), van de Schootbrugge *et al*. (2007) have demonstrated the

potential for oxygen-isotope and Mg/Ca analyses of the oysters from St Audrie's Bay to indicate palaeo-seawater temperature, in this case documenting a temperature increase coincident with a shift to lighter carbon-isotope values over some *c*. 3.5 m of strata. Herein, oxygen-isotope and elemental concentration data are presented for well-preserved low-Mg-calcite oysters for three sections in SW Britain spanning the T–J boundary. These new records greatly extend the dataset from the St Audrie's Bay section (van de Schootbrugge *et al*. 2007) both in terms of quantity and temporal range.

Geological setting

Oysters have been collected at the highest level of stratigraphic resolution possible from the upper Lilstock Formation and lower Blue Lias Formation at Lavernock Point, Glamorgan, South Wales (Fig. 1; Table 1), as well as from St Audrie's Bay and Watchet, Somerset, SW England. The lithostratigraphy of these sections has been described by Richardson (1905, 1911), Whittaker (1978), Whittaker & Green (1983), Waters & Lawrence (1987), Hesselbo *et al*. (2004) and Hounslow *et al*. (2004). Lavernock Point represents the best location to obtain oysters at a high resolution across the T–J interval and through lower Hettangian strata. This section is biostratigraphically well calibrated (Trueman 1920; Hodges 1994) and is easily compared with the succession at St Audrie's Bay where the $\delta^{13}C_{org}$ curve of Hesselbo *et al*. (2002) was generated. Additionally, whole-rock carbonates were sampled from the Pinhay Bay section, near Lyme Regis (Devon, SW England; Fig. 1). The stratigraphy of this section has been described by Richardson (1906), Lang (1924), Hallam (1960*a*), Hesselbo & Jenkyns (1995), Wignall (2001*a*) and Hesselbo *et al*. (2004).

Materials and methods

Although it was not possible in every case to identify the genus and/or species of the sampled shell fragments, most probably all isotope data originate from *Liostrea hisingeri* Nilsson because this form is the only oyster described from the sampled levels (Richardson 1905; Trueman 1920; Hodges, pers. comm.). Oyster shells consist generally of an outer simple prismatic layer and a prominent inner foliated layer (Carter 1990; Hautmann 2006). Both layers consist, at least for Jurassic oysters, primarily of calcite and, particularly in the case of foliated layers, of low-Mg calcite (LMC). Aragonitic elements may also have been present in some oyster shells, but their expression appears to have been suppressed after the earliest Jurassic (Hautmann 2006). In the present study, only material from the foliated layers was analysed.

It is thought that bivalves secrete their shells extracellularly (Lowenstam & Weiner 1989), although studies of artificially damaged specimens of the modern oyster *Crassostrea virginica* (Gmelin) have shown that living hemocytes are present during the rapid growth of prismatic and foliated LMC layers during

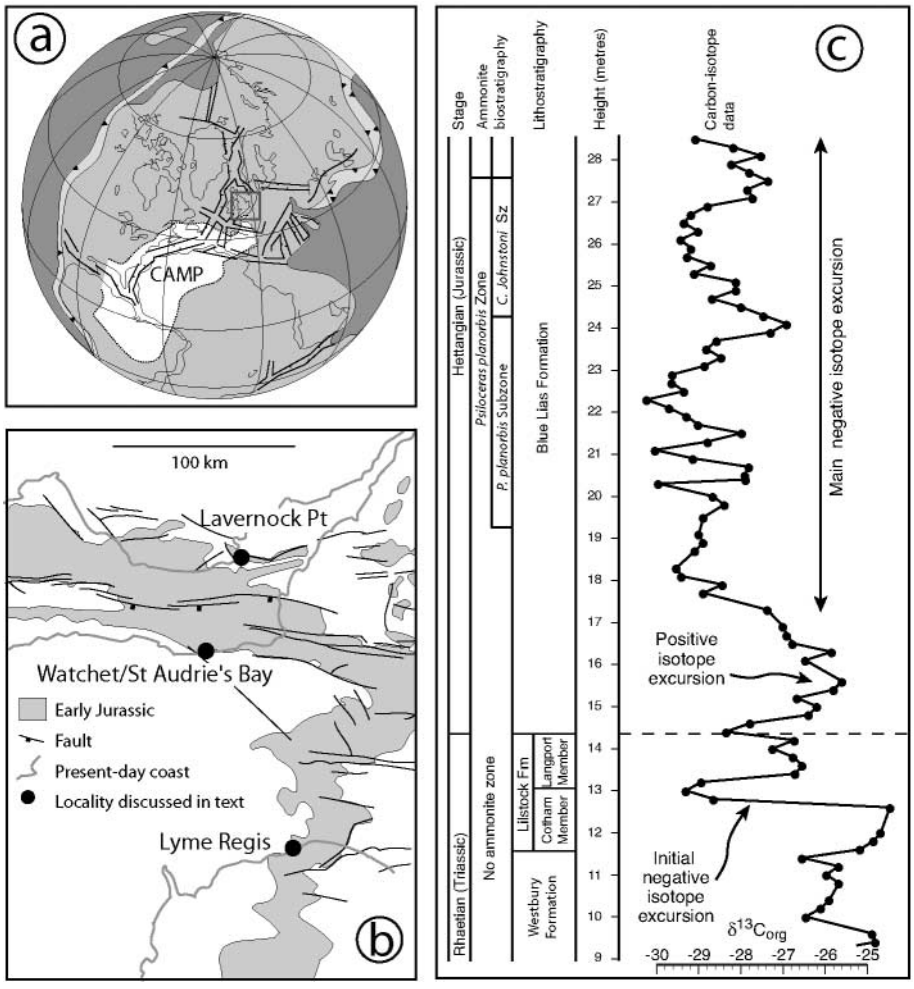

Fig. 1. (**a**) Triassic–Jurassic palaeogeography (modified from Ziegler 1990; McHone 2000; Hesselbo *et al*. 2002). CAMP, Central Atlantic Magmatic Province. White square indicates UK study area. (**b**) Location map for Lavernock Point, Watchet, St Audrie's Bay, and Lyme Regis (modified after Hesselbo *et al*. 2004). (**c**) Summary of pre-existing bulk organic matter carbon-isotope data from St Audrie's Bay (Hesselbo *et al*. 2002) showing the principal features discussed in the text. T–J boundary is positioned on the basis of correlation using carbon isotopes with the proposed GSSP at Kuhjoch, Austria (details provided by Hillebrandt, pers. comm.).

regeneration (Mount *et al*. 2004), a phenomenon that could be intracellular. However, whatever the nature of the process involved, it has been observed that *C. virginica* precipitates the prismatic and foliated shell layers close to oxygen- and carbon-isotope equilibrium with ambient water (Surge *et al*. 2001).

Low-Mg calcite is relatively resistant to diagenetic alteration, thus minimizing the potential resetting of the primary geochemical signal from seawater (e.g. Veizer *et al*. 1997*a*,*b*, 1999; Jenkyns *et al*. 2002). Observed $\delta^{18}O$ and $\delta^{13}C$ variations for modern (Andrus & Crowe 2000; Surge *et al*. 2001) and ancient (Kirby *et al*. 1998; Kirby 2000) oysters reflect climatic and/or environmental changes. Despite the inherent resistance of low-Mg calcite to post-depositional alteration, in the present study each oyster was screened by chemical and optical techniques. The methods used include optical microscopy, scanning electron microscopy (SEM) and elemental analysis by inductively coupled plasma-atomic emission spectroscopy (ICP-AES). The textural observations and elemental data have been utilized to evaluate the isotopic data.

Oysters were prepared by flaking shell fragments using a needle. Splinters of the foliated layers were inspected and handpicked under a binocular microscope. Weathered fragments, attached sedimentary grains, and crack fillings were rejected. Optically well-preserved shell material was checked by SEM to obtain information on microstructural characteristics. Only foliated shell layers with smooth surfaces were regarded as being well preserved. The preservation of foliated structure indicates that post-depositional dissolution and reprecipitation were negligible (Fig. 2).

The Sr and Mn elemental concentrations (Table 1) were determined at the Ruhr-University Bochum by ICP-AES, either on aliquots of phosphoric acid remaining after reaction of shell splinters for evolution of CO_2 (GasBench method), or on additional separated shell splinters generated during sample preparation for the isotope work (Prism II method). International limestone standard reference materials (CCH-1, GBW 03105) were analysed for Sr and Mn along with the samples, and the accuracy and precision of these elemental analyses was better than 3% and 1%, respectively. Obtained Sr and Mn concentrations were utilized to evaluate the pristine preservation of LMC shell material (Brand & Veizer 1980). Although variations of these elements exist for palaeo-seawater throughout the Phanerozoic (Steuber & Veizer 2002), and are concentrated to different degrees in modern bivalves (Vander Putten *et al*. 2000), the content of Sr and Mn provide further information regarding the degree of preservation of the shells. With increasing diagenetic influence, Sr is removed and Mn is added (Brand & Veizer 1980). To be consistent with a number of previous studies (Korte *et al*. 2003, 2005*a*,*b*, 2006, 2008), samples with less than 400 $\mu g\,g^{-1}$ Sr and/or more than 250 $\mu g\,g^{-1}$ Mn were classified as being altered, and their $\delta^{18}O$ values are considered suspect. It should be emphasized that none of the selection criteria are perfectly reliable and the use of only one criterion (e.g. trace-element concentrations) might be misleading when evaluating the extent of alteration. The final evaluation of samples as either pristine or altered was therefore based on optical and microstructural criteria, as well as trace-element chemistry (Table 1). Only carbon- and oxygen-isotope data from well-preserved oysters will be considered in the following presentation, discussion and interpretation.

Samples of about 2 mg of shell fragments (oysters) or fine-grained carbonate (whole rocks) were analysed isotopically for $\delta^{18}O$ and $\delta^{13}C$ at the Department of Earth Sciences, University of Oxford, using a VG Isogas Prism II mass spectrometer with an on-line VG Isocarb common acid-bath preparation system. In the instrument, the powdered sample is reacted with purified phosphoric acid (H_3PO_4) at 90 °C. Calibration to the V-PDB standard via NBS-19 is made daily using the Oxford in-house (NOCZ) Carrara Marble standard. Reproducibility of replicated standards is typically better than 0.1‰ for $\delta^{13}C$ and $\delta^{18}O$.

Single shell splinters (<0.5 mm) with a mass of about 0.1 mg were prepared in *c*. 1 mm steps in the growth direction for six well-preserved oysters from the Lavernock Point section to examine intra-shell variation in $\delta^{13}C$ and $\delta^{18}O$ values. Surface layers were removed and sampling started about 1 mm below the surface. These considerably smaller samples were analysed for $\delta^{18}O$ and $\delta^{13}C$ on a GasBench II linked to a ThermoFinnigan Delta^{plus}XL mass spectrometer at the Institut für Geologie und Paläontologie of the Universität Innsbruck (Spötl & Vennemann 2003). The long-term precision (1 s.d.) is better than 0.06‰ for $\delta^{13}C$ and better than 0.08‰ for $\delta^{18}O$. Carbon- and oxygen-isotope values were calibrated against V-PDB and are reported in the standard ‰ notation (Tables 1 and 2).

Some carbonate samples (Table 1; *c*. 0.2 mg) were analysed at the Institut für Geologie, Mineralogie und Geophysik, Ruhr-Universität Bochum also using a GasBench II linked to a ThermoFinnigan Delta S mass spectrometer. The results from the carbonate samples were corrected to the nominal values for the carbon- and oxygen-isotope standards CO-1 and CO-8. Reproducibility was better than 0.1‰ for both $\delta^{13}C$ and $\delta^{18}O$. Carbon- and oxygen-isotope values were calibrated against V-PDB and are reported in the standard ‰ notation (Table 1). Tests in all three laboratories demonstrated that NBS-19 and NOCZ showed similar results and are within ±0.1‰ for both $\delta^{13}C$ and $\delta^{18}O$.

Shell splinters of about 0.25 mg were powdered for the Mg/Ca ratio measurements. To be consistent with previous work, the samples were cleaned by a procedure developed and revised by Boyle & Keigwin (1985) whereby ferromanganese oxides and organic matter were removed (see Rickaby & Halloran 2005). After a weak acid leach (0.001M HNO_3), the samples were dissolved in 0.5 ml 0.22M HNO_3 and centrifuged for 5 min at 5000 r.p.m. Analysis was carried out by inductively coupled plasma-mass spectrometry (ICP-MS) at Oxford University, using a PerkinElmer PESCIEX ELAN 6100 DRC Quadrupole ICP-MS system fed by a low-uptake (100 $\mu l\ min^{-1}$) spray-chamber nebulizer (see Rosenthal *et al*. 1999). Data were collected for four masses: ^{46}Ca, ^{26}Mg, ^{88}Sr, and ^{55}Mn with the ICP-MS system set to peak hopping mode using a method adapted from Harding *et al*. (2006).

Results

Carbon and oxygen isotopes

Most of the oysters originate from the Lavernock Point section (Fig. 1) and, for this locality, the lithology, stratigraphy, and oxygen- and carbon-isotope data are shown in Figure 3. The lowest well-preserved oysters retrieved originated from the lower Langport Member and collection was continued up through the Langport Member and the Blue Lias Formation, the latter including the *P. planorbis*, *C. johnstoni* and the *W. portlocki* ammonite subzones of the *P. planorbis* and *A. liasicus* ammonite zones of the Hettangian (Fig. 3). The lowest well-preserved oysters originated from the base of Bed A, from the lower Langport Member. A correlation from Lavernock to the proposed Global Stratotype and Stratigraphic Point (GSSP) at Kujoch, Austria (Hillebrandt, pers. comm.), cannot be accomplished on the basis of biostratigraphy because the UK sections lack

Table 1. *Positions, material analysed, carbon- and oxygen-isotope values, Mg/Ca and Sr/Ca ratios, and Mn and Sr concentrations of the analysed samples*

Sample	Height above base Langport Mbr (cm)	Material	$\delta^{13}C$ (‰ V-PDB)	$\delta^{18}O$ (‰ V-PDB)	Isotope laboratory	Mg/Ca (mM M^{-1})	Sr/Ca (mM M^{-1})	Mn (μg g^{-1})	Sr (μg g^{-1})
Pristine oysters									
LAV 109	36	Oyster	2.87	−0.42	Ox	9.03	0.58	237	431
LAV 109	36	Oyster	3.30	0.46	Bo	8.42	0.55	237	431
LAV 109 b	36	Oyster	3.00	−0.39	Ox	nd	nd	237	431
LAV 109	36	Oyster	3.76	−0.18	Inn	nd	nd	237	431
LAV 110	91	Oyster	2.24	−0.09	Bo	5.08	0.55	242	570
LAV 110	91	Oyster	2.89	−0.12	Ox	5.44	0.63	242	570
LAV 261	91	Oyster	3.18	0.88	Bo	4.08	0.55	126	597
LAV 110-1	91	Oyster	2.83	−0.10	Inn	4.98	0.55	216	472
LAV 110-1	91	Oyster	2.86	−0.34	Inn	7.10	0.55	216	472
LAV 261	91	Oyster	3.36	0.96	Inn	4.03	0.52	126	597
LAV 261	91	Oyster	3.29	0.55	Inn	4.13	0.57	126	597
LAV 257	171	Oyster	3.51	0.19	Bo	nd	nd	174	530
LAV 257	171	Oyster	3.55	−0.12	Bo	nd	nd	174	530
LAV 258	171	Oyster	4.63	1.62	Bo	2.28	0.48	126	570
LAV 257	171	Oyster	3.94	0.04	Inn	nd	nd	174	530
LAV 262	275	Oyster	3.62	−0.49	Bo	nd	nd	80	560
LAV 262	275	Oyster	4.11	0.35	Bo	5.50	0.56	44	538
LAV 264	285	Oyster	3.62	0.08	Bo	nd	nd	81	482
LAV 204	290	Oyster	4.04	−0.05	Bo	4.69	0.55	185	585
LAV 204	290	Oyster	4.04	−0.05	Bo	6.29	0.50	185	585
LAV 204	290	Oyster	4.04	−0.05	Bo	5.39	0.57	185	585
LAV 204	290	Oyster	4.04	−0.05	Bo	6.29	0.50	185	585
LAV 203-1	303	Oyster	3.02	0.17	Bo	nd	nd	32	518
LAV 203-1	303	Oyster	3.31	0.02	Ox	nd	nd	32	518
LAV 200	332	Oyster	4.34	−0.81	Ox	11.57	0.69	57	646
LAV 200	332	Oyster	4.53	−0.65	Bo	9.92	0.61	57	646
LAV 201	332	Oyster	4.77	−1.02	Ox	4.48	0.52	53	608
LAV 200	332	Oyster	4.45	−0.36	Inn	5.23	0.56	57	646
LAV 205	362	Oyster	3.68	−0.87	Ox	nd	nd	83	515
LAV 206	403	Oyster	3.88	−0.80	Ox	6.87	0.52	64	465
LAV 206	403	Oyster	3.88	−0.80	Ox	13.33	0.62	64	465
LAV 207-1	403	Oyster	3.69	−0.66	Ox	9.56	0.53	48	576
LAV 207-2	403	Oyster	4.00	−0.34	Bo	8.55	0.54	64	566
LAV 207-2	403	Oyster	4.16	−0.48	Ox	nd	nd	64	566
LAV 207-1	403	Oyster	2.93	−1.06	Inn	5.59	0.55	48	576
LAV 208	425	Oyster	4.25	0.22	Bo	6.55	0.50	31	594
LAV 209	448	Oyster	2.98	−0.93	Ox	nd	nd	189	547
LAV 210-1	451	Oyster	3.33	−1.17	Ox	6.34	0.46	128	531
LAV 210-1	451	Oyster	3.33	−1.17	Ox	7.89	0.51	128	531
LAV 210-2	451	Oyster	3.43	−1.09	Inn	5.43	0.50	67	496
LAV 210-2	451	Oyster	3.55	−1.18	Ox	nd	nd	67	496
LAV 218	477	Oyster	3.17	−1.25	Bo	5.63	0.50	93	574
LAV 218	477	Oyster	3.38	−1.18	Ox	nd	nd	93	574
LAV 212	497	Oyster	3.26	−0.38	Ox	7.62	0.52	50	580
LAV 212	497	Oyster	3.26	−0.38	Ox	9.59	0.58	50	580
LAV 220	500	Oyster	3.95	−0.82	Ox	nd	nd	41	537
LAV 213-1	515	Oyster	2.54	−0.43	Bo	nd	nd	75	527
LAV 213-3	515	Oyster	3.24	−0.24	Bo	5.39	0.46	44	965
LAV 214-2	526	Oyster	3.51	−0.27	Ox	5.73	0.51	17	498
LAV 214-2	526	Oyster	3.52	0.16	Inn	4.65	0.51	17	498
LAV 215-1	537	Oyster	2.76	−0.46	Ox	nd	nd	37	480
LAV 215-2	537	Oyster	3.02	−0.54	Ox	7.44	0.51	53	501
LAV 215-2	537	Oyster	3.02	−0.54	Ox	9.23	0.54	53	501
LAV 216	605	Oyster	2.93	−1.19	Bo	nd	nd	15	638
LAV 216	605	Oyster	3.07	−1.05	Inn	6.07	0.55	15	638
LAV 217-1	624	Oyster	2.15	−1.79	Ox	4.30	0.56	29	583
LAV 217-1	624	Oyster	2.51	−1.25	Bo	5.76	0.63	29	583
LAV 219	648	Oyster	2.45	−0.69	Inn	5.77	0.54	110	434
LAV 232	877	Oyster	2.16	−1.09	Bo	nd	nd	5	506
LAV 232	877	Oyster	1.86	−1.06	Inn	3.96	0.51	5	506
LAV 230	882	Oyster	2.36	−1.78	Bo	nd	nd	52	517
LAV 233	898	Oyster	1.99	−1.74	Bo	nd	nd	10	590
LAV 235-A	968	Oyster	1.71	−0.97	Bo	nd	nd	15	500
LAV 235-B	968	Oyster	2.01	−0.06	Bo	nd	nd	46	430
LAV 237	1102	Oyster	2.48	−0.99	Bo	nd	nd	21	461

(*continued*)

Table 1. (*continued*)

Sample	Height above base Langport Mbr (cm)	Material	$\delta^{13}C$ (‰ V-PDB)	$\delta^{18}O$ (‰ V-PDB)	Isotope laboratory	Mg/Ca (mM M^{-1})	Sr/Ca (mM M^{-1})	Mn (μg g^{-1})	Sr (μg g^{-1})
LAV 238	1102	Oyster	1.69	−1.46	Bo	nd	nd	84	449
LAV 237	1102	Oyster	1.73	−1.12	Inn	9.14	0.53	21	461
LAV 243	1239	Oyster	2.04	−0.89	Bo	nd	nd	80	456
LAV 244	1249	Oyster	2.73	−1.52	Bo	nd	nd	48	607
LAV 246	1473	Oyster	2.59	−1.41	Bo	nd	nd	16	480
LAV 246	1473	Oyster	2.78	−1.26	Inn	3.43	0.55	16	480
LAV 247	1552	Oyster	2.32	−2.05	Bo	nd	nd	173	560
LAV 249	1708	Oyster	1.61	−2.03	Bo	nd	nd	84	433
LAV 249	1708	Oyster	2.01	−1.24	Bo	nd	nd	89	425
LAV 256	1748	Oyster	1.26	−1.79	Bo	nd	nd	127	466
LAV 255-C	1781	Oyster	1.89	−1.88	Bo	nd	nd	190	520
LAV 255-C	1781	Oyster	1.98	−1.39	Inn	2.91	0.55	190	520
LAV 252	2075	Oyster	1.37	−1.98	Bo	nd	nd	103	525
LAV 251-A	2080	Oyster	1.82	−1.81	Bo	nd	nd	180	480
LAV 251-B	2080	Oyster	1.70	−2.23	Bo	nd	nd	61	500
SAB 165-1	415	Oyster	2.23	−1.29	Ox	5.14	0.45	7	471
Wa 1	285	Oyster	3.64	−0.71	Ox	nd	nd	49	550
Wa 2	325	Oyster	3.22	−0.35	Ox	8.69	0.52	57	574
Altered oysters									
LAV 107-1	4	Oyster	0.59	−1.45	Ox	nd	nd	1373	687
LAV 210-3	451	Oyster	3.19	−1.31	Ox	nd	nd	nd	nd
LAV 211	470	Oyster	4.06	−0.10	Ox	nd	nd	440	570
LAV 213-2	515	Oyster	2.03	−2.03	Bo	nd	nd	338	411
LAV 214-1	526	Oyster	2.20	−1.00	Bo	nd	nd	227	386
LAV 231	885	Oyster	2.25	−1.49	Bo	nd	nd	nd	nd
LAV 245-B	1473	Oyster	2.37	−1.17	Bo	nd	nd	53	388
LAV 255-B	1781	Oyster	1.80	−1.62	Bo	nd	nd	267	519
SAB 100-1	(below) −265	Oyster	−2.72	−2.76	Ox	nd	nd	1636	1100
SAB 100-2	(below) −265	Oyster	−4.11	−3.68	Ox	nd	nd	1392	681
SAB 179	(below) −1115	Oyster	−3.49	−10.35	Bo	nd	nd	817	463
Wa BBL	0	Oyster	−5.59	−6.22	Ox	nd	nd	743	347
Bulk rocks									
LAV 110-1	91	Bulk rock	−0.43	−5.19	Bo	nd	nd	nd	nd
LAV 210	451	Bulk rock	0.87	−4.67	Bo	nd	nd	nd	nd
LAV 201	332	Bulk rock	−0.10	−5.19	Bo	nd	nd	nd	nd
LAV 219	648	Bulk rock	0.77	−3.50	Bo	nd	nd	nd	nd

LAV, Lavernock Point; SAB, St Audrie's Bay; Wa, Watchet; Ox, Oxford; Bo, Bochum; Inn, Innsbruck; nd, not determined.

relevant ammonites. However, on the basis of the carbon-isotope data available from St Audrie's Bay, together with the new data presented here, the T–J boundary should lie within the Langport Member at Lavernock.

The general trend in $\delta^{13}C$ values through the Lavernock Point section is marked by a prominent positive excursion, which starts from *c*. 3‰ in the lower Langport Member, increasing by about 2‰ to highest values of *c*. 5‰ in the lower Blue Lias, followed by a 3‰ decrease to *c*. 2‰ just below the base of the *planorbis* Zone (Fig. 3). The carbon-isotope values remain relatively low up to the *portlocki* Subzone of the *liasicus* Zone (with slight variations in the *johnstoni* Zone).

Highly resolved $\delta^{13}C$ profiles in the growth directions of the shells for six well-preserved oysters from Lavernock Point are shown in Figure 4 and Table 2: two of these samples were also profiled perpendicular to growth direction. Carbon-isotope values show a range of about 1‰ in LAV 110 (mean: 2.8 ± 0.2‰, $n = 44$), less than 1‰ in LAV 258 (mean: 4.5 ± 0.2‰, $n = 8$), about 0.6‰ in LAV 201 (mean: 4.9 ± 0.2‰, $n = 8$), more than 1.1‰ in LAV 208 (mean: 3.8 ± 0.4‰, $n = 8$), nearly 1.3‰ in LAV 210 (mean: 3.5 ± 0.3‰, $n = 26$) and about 1.4‰ in LAV 219 (1.8 ± 0.4‰, $n = 28$). The $\delta^{13}C$ values perpendicular to the growth direction vary much less: about 0.6‰ in both LAV 201 (mean: 4.9 ± 0.2‰, $n = 7$) and LAV 210 (mean: 3.6 ± 0.1‰, $n = 16$).

Carbon-isotope values from the Lyme Regis section (Fig. 5; Table 3), based on analysis of whole-rock carbonate, are about 3 ± 0.5‰ within the lower Langport Member. A decrease in values of these samples starts in the upper Langport Member, falling to about 1‰ just below the base of the *planorbis* Zone. This declining trend continues, reaching −0.2‰ at the top of the *planorbis* Subzone. The carbon-isotope values remain low (*c*. 0‰) in the *johnstoni* and *portlocki* Subzones, but it should be noted that only one $\delta^{13}C$ value was obtained for each of these two units.

The $\delta^{18}O$ values from Lavernock Point oysters are about 0‰ (±1‰) in the lower Langport Member, increase somewhat to highest values of more than 1.6‰ in the upper Langport Member and decline sharply (with some reversals) to values of about −2‰ in the *portlocki* Subzone of the Blue Lias Formation. The $\delta^{18}O$ variations in shell-growth direction and perpendicular-to-growth direction of each of the six well-preserved oysters show the features described below (Fig. 4, Table 2). The oxygen-isotope values vary by about 2.1‰ in LAV 110 (mean: −0.2 ± 0.5‰, $n = 44$), by more than 2‰ in LAV 258 (mean: +0.6 ± 0.9‰, $n = 8$), by only 0.2‰ in LAV 201 (mean: −1.0 ± 0.1‰, $n = 8$), by about 1.1‰ in LAV 208 (mean: −0.3 ± 0.4‰, $n = 8$), by 0.7‰ in LAV 210 (mean: −1.0 ± 0.2‰, $n = 26$) and by more than 1.6‰ in LAV 219 (−1.5 ± 0.5‰, $n = 28$). The $\delta^{18}O$ variations perpendicular to the growth direction are 0.2‰

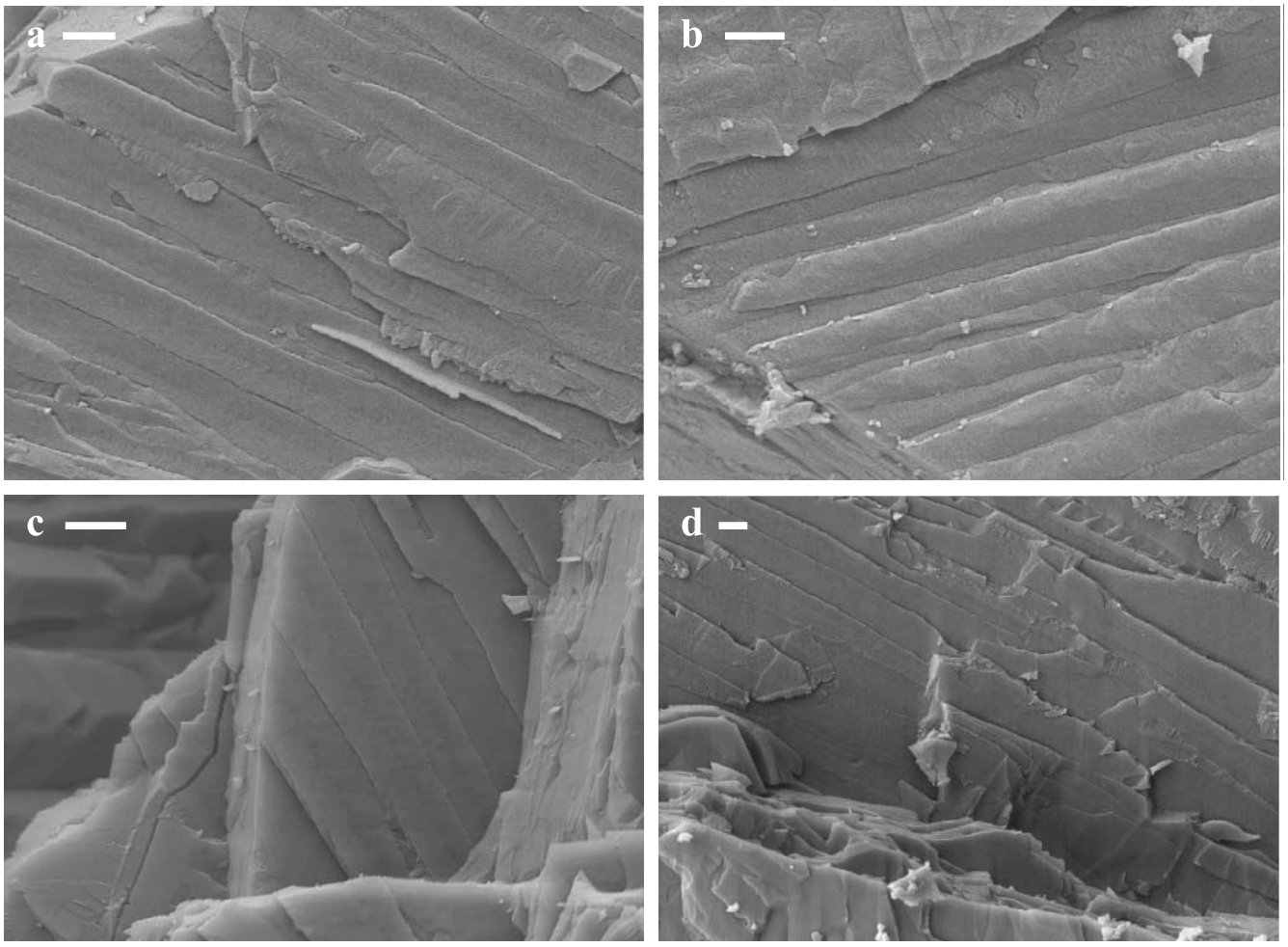

Fig. 2. SEM images of well-preserved foliated layers of oyster shells. (**a**) LAV 110; (**b**) LAV 204; (**c**) LAV 219; (**d**) LAV 251. Scale bars represent 2 μm.

in LAV 201 (mean: -0.9 ± 0.1‰, $n = 7$) and more than 0.4‰ in LAV 210 (mean: -1.2 ± 0.1‰, $n = 16$).

To aid discussion of the oxygen- and carbon-isotope trends, all $\delta^{13}C$ and $\delta^{18}O$ values from well-preserved oysters at Lavernock Point and from the St Audrie's Bay area (including the previously published data of van de Schootbrugge *et al*. (2007)) are compiled in Figure 6, together with the whole-rock carbonate $\delta^{13}C$ data from the Lyme Regis section.

The isotopic values of well-preserved oyster shells collected from the same stratigraphic level, and therefore geologically coeval, show spreads of more than 1‰ for both $\delta^{13}C$ and $\delta^{18}O$ (Figs 3, 4 and 6). Such variation is also seen in single shells and is the norm for modern oysters (Surge *et al*. 2001), reflecting seasonal environmental and temperature change. Therefore, when discussing long-term changes in environmental parameters, the general trends enclosed in the envelopes shown in Figure 6 should be considered. It should be noted that the scatter of carbon- and oxygen-isotope values for the six oysters fit perfectly within the general trends, constituting evidence that both $\delta^{13}C$ and $\delta^{18}O$ values represent a primary seawater signal.

Mg/Ca and Sr/Ca ratios

Mg/Ca and Sr/Ca ratios have been generated for 48 well-preserved oyster shells (Table 1) and these vary in the range 2.3–13.3 mmol mol^{-1} and 0.4–0.7 mmol mol^{-1}, respectively. It has been reported that Mg and Sr concentrations in bivalve shells depend on ambient seawater temperature and increase with warming (Dodd 1965; see also Stecher *et al*. 1996). Notably, Klein *et al*. (1996*a*) documented that for the modern bivalve *Mytilus trossulus* (Gould) the Mg/Ca ratios tend to reach higher values with rising seawater temperature. However, in a more extensive study Vander Putten *et al*. (2000) found that Mg/Ca ratios in *Mytilus edulis* (Linnaeus) shell calcite showed considerable deviations from those expected from water temperature alone, implying that metabolic processes are involved in Mg incorporation into the calcite framework. For strontium also it is most likely that water temperature is not the unique control on the Sr/Ca ratios in bivalve shells because, in modern bivalves, metabolic or kinetic effects and/or seawater chemistry have also been shown to be important (Klein *et al*. 1996*b*; Vander Putten *et al*. 2000; Lorrain *et al*. 2005). Work on other modern bivalve groups has added further weight to the view that their Mg/Ca and Sr/Ca ratios are unreliable palaeotemperature proxies (Freitas *et al*. 2006).

The temperature dependence of Mg/Ca and Sr/Ca ratios in Early Jurassic oysters was assessed by plotting these ratios against $\delta^{18}O$ (Fig. 7), a procedure that assumes that $\delta^{18}O$ is overwhelmingly controlled by seawater temperature (discussed further below). There are no significant correlations, and there-

Table 2. *Highly resolved* $\delta^{13}C$ *and* $\delta^{18}O$ *profiles of six well-preserved* Liostrea *samples*

Sample	Section	Direction	Distance (mm)	$\delta^{13}C$ (‰ V-PDB)	$\delta^{18}O$ (‰ V-PDB)
LAV 110-1	1	Grow.	0.50	3.13	0.34
LAV 110-1	1	Grow.	1.25	3.13	0.83
LAV 110-1	1	Grow.	1.90	2.96	0.46
LAV 110-1	1	Grow.	8.25	2.89	−0.58
LAV 110-1	1	Grow.	8.71	2.56	−1.26
LAV 110-1	1	Grow.	9.14	3.07	−0.24
LAV 110-1	1	Grow.	9.14	3.12	−0.14
LAV 110-1	1	Grow.	9.48	3.08	−0.07
LAV 110-1	1	Grow.	9.56	3.11	−0.14
LAV 110-1	1	Grow.	9.86	3.05	−0.40
LAV 110-1	1	Grow.	10.20	2.91	−0.14
LAV 110-1	1	Grow.	10.97	3.04	−0.26
LAV 110-1	1	Grow.	11.48	3.00	−0.48
LAV 110-1	1	Grow.	11.90	2.56	−0.39
LAV 110-1	1	Grow.	12.45	2.39	−0.59
LAV 110-1	1	Grow.	12.96	2.43	−0.40
LAV 110-1	1	Grow.	13.73	2.74	0.26
LAV 110-1	1	Grow.	14.24	2.82	0.37
LAV 110-1	1 (b)	Grow.	1.80	2.93	0.54
LAV 110-1	1 (b)	Grow.	5.00	2.72	−0.20
LAV 110-1	1 (b)	Grow.	6.15	2.99	−0.45
LAV 110-1	1 (b)	Grow.	6.25	2.81	−0.16
LAV 110-1	1 (b)	Grow.	7.25	2.88	−0.76
LAV 110-1	1 (b)	Grow.	9.27	2.85	−0.46
LAV 110-1	1 (b)	Grow.	10.29	2.61	−0.69
LAV 110-1	1 (b)	Grow.	10.75	2.96	−0.55
LAV 110-1	1 (b)	Grow.	11.01	2.49	−0.29
LAV 110-1	1 (b)	Grow.	11.65	2.35	−0.12
LAV 110-1	1 (b)	Grow.	12.67	2.44	−0.53
LAV 110-1	1 (b)	Grow.	13.43	2.79	0.49
LAV 110-1	1 (b)	Grow.	13.81	2.76	0.86
LAV 110-1	2	Grow.	0.85	2.82	0.24
LAV 110-1	2	Grow.	1.75	2.98	0.54
LAV 110-1	2	Grow.	2.65	2.26	0.77
LAV 110-1	2	Grow.	3.65	2.57	−0.01
LAV 110-1	2	Grow.	5.15	2.74	−0.65
LAV 110-1	2	Grow.	5.30	2.83	−0.69
LAV 110-1	2	Grow.	6.10	2.83	−0.58
LAV 110-1	2	Grow.	6.50	2.96	−0.02
LAV 110-1	2	Grow.	7.40	2.87	−0.31
LAV 110-1	2	Grow.	7.65	2.63	−0.50
LAV 110-1	2	Grow.	8.50	2.97	−0.07
LAV 110-1	2	Grow.	10.50	2.71	−0.04
LAV 110-1	2	Grow.	11.50	2.25	−0.39
LAV 201	1	Grow.	0.75	4.74	−0.94
LAV 201	1	Grow.	1.40	4.65	−1.05
LAV 201	1	Grow.	1.80	4.55	−1.01
LAV 201	1	Grow.	2.75	4.92	−0.92
LAV 201	1	Grow.	4.25	4.89	−0.98
LAV 201	1	Grow.	4.50	5.14	−0.89
LAV 201	1	Grow.	5.10	4.95	−1.08
LAV 201	1	Grow.	6.05	5.05	−0.87
LAV 201	2	Perp.	0.80	5.07	−0.79
LAV 201	2	Perp.	2.20	4.69	−1.02
LAV 201	2	Perp.	3.75	4.50	−0.99
LAV 201	2	Perp.	3.90	4.98	−0.89
LAV 201	2	Perp.	5.05	4.99	−0.82
LAV 201	2	Perp.	6.00	4.83	−0.84
LAV 201	2	Perp.	7.50	5.05	−0.81
LAV 208-p	1	Grow.	3.50	3.56	−0.57
LAV 208-p	1	Grow.	5.50	3.89	−0.46
LAV 208-p	1	Grow.	7.30	3.61	−0.73
LAV 208-p	1	Grow.	9.00	3.62	−0.60
LAV 208-p	1	Grow.	10.00	3.14	−0.56
LAV 208-p	1	Grow.	12.50	3.91	−0.02
LAV 208-p	1	Grow.	14.50	4.18	0.17
LAV 208-p	1	Grow.	17.00	4.26	0.33
LAV 210-2	1	Grow.	0.90	3.78	−0.93
LAV 210-2	1	Grow.	0.90	3.71	−1.31
LAV 210-2	1	Grow.	1.00	3.07	−0.75
LAV 210-2	1	Grow.	2.00	3.46	−1.02
LAV 210-2	1	Grow.	2.50	3.35	−1.21
LAV 210-2	1	Grow.	2.60	3.12	−1.19
LAV 210-2	1	Grow.	3.80	3.46	−0.87
LAV 210-2	1	Grow.	4.40	2.97	−1.15
LAV 210-2	1	Grow.	4.85	3.47	−0.99
LAV 210-2	1	Grow.	4.90	3.04	−1.23
LAV 210-2	1	Grow.	5.80	3.57	−0.92
LAV 210-2	1	Grow.	6.00	4.13	−0.88
LAV 210-2	1	Grow.	7.50	3.85	−0.92
LAV 210-2	1	Grow.	7.50	3.31	−1.00
LAV 210-2	1	Grow.	7.60	3.67	−0.70
LAV 210-2	1	Grow.	8.50	3.82	−0.84
LAV 210-2	1	Grow.	9.50	3.55	−0.98
LAV 210-2	1	Grow.	10.05	4.01	−0.63
LAV 210-2	1	Grow.	11.00	3.63	−0.79
LAV 210-2	1	Grow.	11.30	3.79	−0.96
LAV 210-2	1	Grow.	12.50	3.52	−0.93
LAV 210-2	1	Grow.	12.50	3.70	−1.09
LAV 210-2	1	Grow.	13.60	3.65	−0.92
LAV 210-2	1	Grow.	14.35	2.88	−0.92
LAV 210-2	1	Grow.	14.40	3.54	−0.96
LAV 210-2	1	Grow.	15.50	3.51	−0.96
LAV 210-2	2	Perp.	3.00	3.78	−0.96
LAV 210-2	2	Perp.	4.50	3.69	−1.13
LAV 210-2	2	Perp.	6.00	3.64	−1.13
LAV 210-2	2	Perp.	6.90	3.53	−1.34
LAV 210-2	2	Perp.	8.25	3.52	−1.11
LAV 210-2	2	Perp.	4.50	3.65	−1.14
LAV 210-2	2	Perp.	3.20	3.80	−0.94
LAV 210-2	2	Perp.	3.85	3.74	−1.05
LAV 210-2	2	Perp.	9.20	3.52	−1.08
LAV 210-2	2	Perp.	10.50	3.59	−1.16
LAV 210-2	2	Perp.	11.50	3.48	−1.17
LAV 210-2	2	Perp.	11.10	3.50	−1.25
LAV 210-2	2	Perp.	12.50	3.54	−1.17
LAV 210-2	2	Perp.	13.50	3.55	−1.27
LAV 210-2	2	Perp.	15.15	3.40	−1.03
LAV 210-2	2	Perp.	15.00	3.24	−1.41
LAV 219	1	Grow.	0.80	2.30	−0.93
LAV 219	1	Grow.	1.70	1.64	−2.08
LAV 219	1	Grow.	3.00	1.69	−1.65
LAV 219	1	Grow.	4.25	1.43	−2.30
LAV 219	1	Grow.	5.50	2.63	−0.67
LAV 219	1	Grow.	6.00	1.89	−1.10
LAV 219	1	Grow.	7.30	1.94	−1.56
LAV 219	1	Grow.	6.50	1.56	−1.80
LAV 219	1	Grow.	7.50	2.09	−1.37
LAV 219	1	Grow.	8.50	1.75	−1.82
LAV 219	1	Grow.	9.85	2.43	−1.04
LAV 219	1	Grow.	11.00	1.79	−1.84
LAV 219	1	Grow.	11.50	2.40	−0.84
LAV 219	1	Grow.	13.50	2.40	−0.71
LAV 219	1	Grow.	12.50	2.01	−1.24
LAV 219	2	Grow.	0.85	2.20	−0.71
LAV 219	2	Grow.	1.50	1.51	−1.32
LAV 219	2	Grow.	2.60	1.43	−1.84
LAV 219	2	Grow.	3.50	1.38	−2.07
LAV 219	2	Grow.	5.50	1.57	−1.62
LAV 219	2	Grow.	6.50	1.28	−1.82
LAV 219	2	Grow.	4.50	1.31	−2.21
LAV 219	2	Grow.	7.50	1.36	−1.94
LAV 219	2	Grow.	8.50	1.24	−1.95
LAV 219	2	Grow.	9.50	1.70	−1.44
LAV 219	2	Grow.	10.50	1.82	−1.17
LAV 219	2	Grow.	11.50	2.34	−0.73
LAV 219	2	Grow.	12.50	2.30	−0.86
LAV 258	1	Grow.	4.50	4.89	1.64
LAV 258	1	Grow.	6.50	4.69	1.45
LAV 258	1	Grow.	7.50	4.46	1.36
LAV 258	1	Grow.	8.50	4.58	0.89
LAV 258	1	Grow.	14.50	4.29	0.23
LAV 258	1	Grow.	15.00	4.18	0.11
LAV 258	1	Grow.	22.50	4.47	−0.43
LAV 258	1	Grow.	24.50	4.21	−0.52

Grow., growth direction; Perp., perpendicular to growth direction.

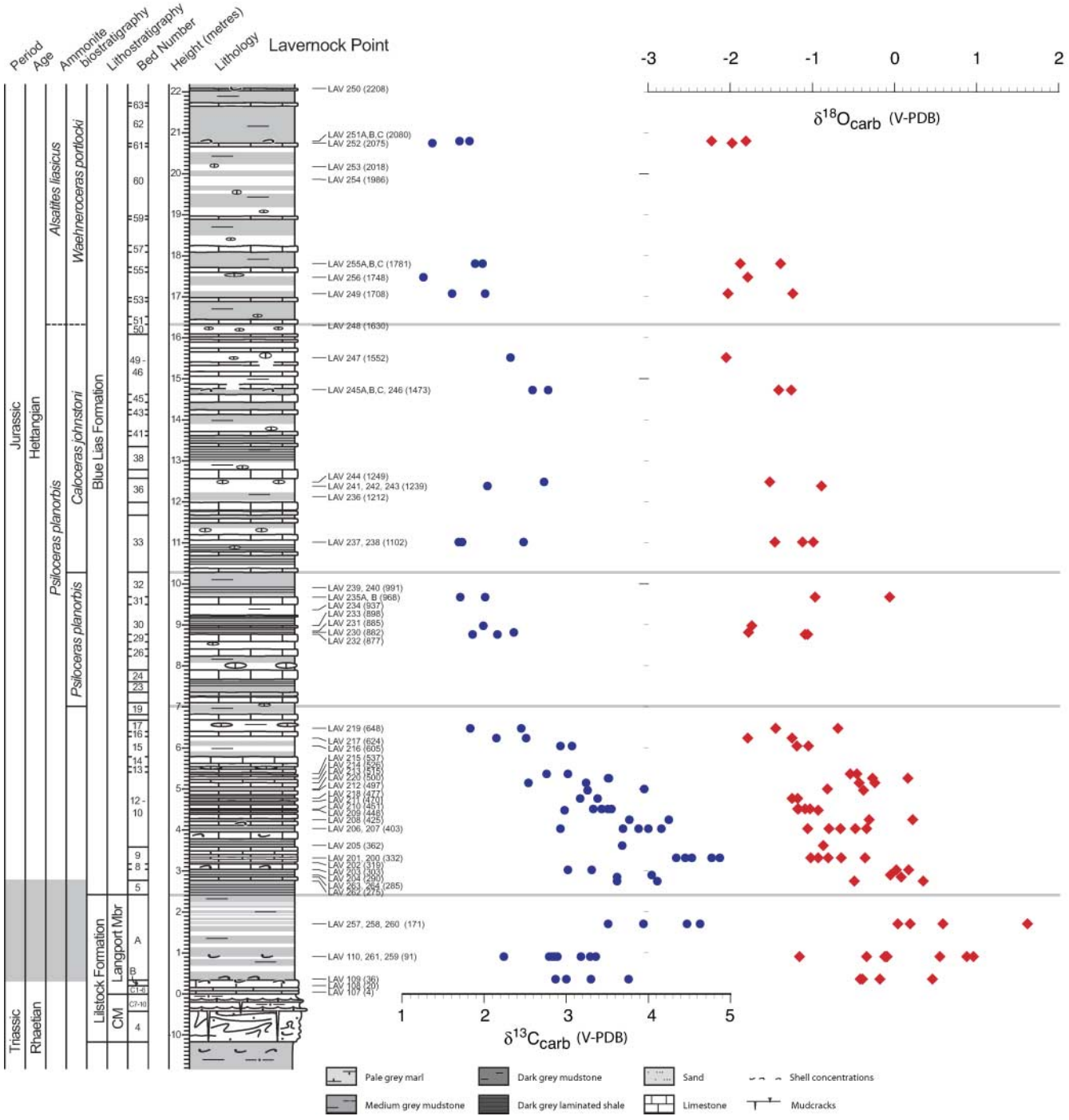

Fig. 3. Stratigraphic section for Lavernock Point, showing sample locations and carbon- and oxygen-isotope values for well-preserved oyster (*Liostrea*) shell calcite. T–J boundary position is less precisely definable in comparison with St Audrie's Bay, but on the basis of carbon-isotope stratigraphy must lie somewhere within the marly upper beds of the Langport Member.

fore it can be inferred that Mg/Ca and Sr/Ca ratios of the investigated Mesozoic *Liostrea hisingeri* are determined mainly by factors other than temperature. It is notable that these results are in contrast to those of van de Schootbrugge *et al*. (2007), who reported a distinct increase of oyster-calcite Mg/Ca and Sr/Ca ratios with decreasing $\delta^{18}O$ values, but this was based on a much smaller dataset.

Discussion

Significance for correlation of T–J boundary strata

Carbon-isotope shifts reflect perturbations in the Earth's carbon cycle at a variety of spatial scales (Kump & Arthur 1999). It is understood that seawater $\delta^{13}C$ is controlled by the burial and re-oxidation of ^{12}C-enriched organic matter within the ocean–

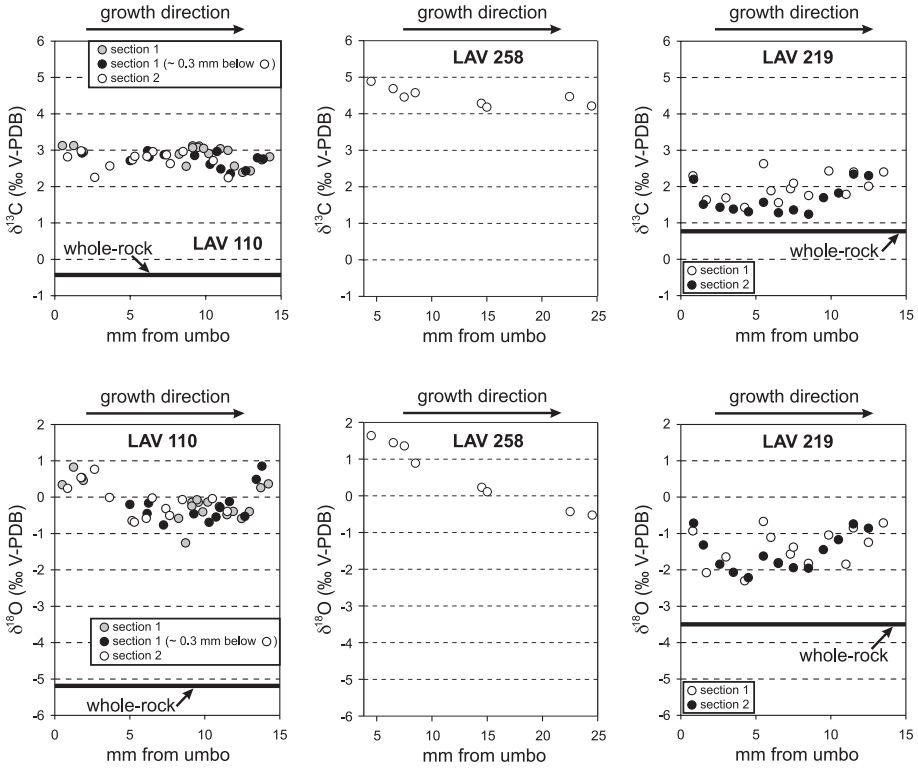

Fig. 4. $\delta^{18}O$ and $\delta^{13}C$ variations of foliated layers in growth direction for three well-preserved *Liostrea* shells. Two cut sections have been analysed from sample LAV 110 (lower Langport Member), and one of these has been sampled for different depths below the surface (section 1: open circles, *c*. 1 mm below the surface; grey circles, *c*. 1.3 mm below the surface). All other sections have been sampled *c*. 1 mm below the surfaces to avoid contamination.

atmosphere system, linked to several factors, such as atmospheric CO_2 levels, nutrient supply, sedimentation rates, net primary productivity, biological isotope fractionation or sea-level changes (Scholle & Arthur 1980; Jenkyns 1996; Hayes *et al*. 1999; Kump & Arthur 1999; Jarvis *et al*. 2006). Additional mechanisms suggested to add significant masses of isotopically light carbon include input of volcanic mantle-derived CO_2 into the ocean–atmosphere system (Hansen 2006), sudden release of methane from gas hydrates (Dickens *et al*. 1997; Hesselbo *et al*. 2000), thermal metamorphism of organic-rich sediments (Svensen *et al*. 2004; McElwain *et al*. 2005) or overturn of ^{12}C-enriched (anoxic) oceanic bottom waters (e.g. Küspert 1982; Knoll *et al*. 1996).

Many carbon-isotope excursions are global in scale, and are registered in a wide range of marine and continental deposits such as platform carbonates, calcareous pelagic sediments, organic-rich shales, terrestrial palaeosols and lacustrine deposits. The coeval nature of the $\delta^{13}C$ fluctuations makes it possible to use the peaks and troughs for trans-continental stratigraphic correlation for many stage boundaries (e.g. Permian–Triassic boundary; Korte & Kozur 2005), and this has also been proposed for the T–J boundary through the correlation of $\delta^{13}C_{org}$ fluctuations of several sections in North America and Europe (Hesselbo *et al*. 2002, 2004; McRoberts *et al*. 2007). The carbon-isotope stratigraphy from the well-preserved oysters from T–J boundary sections presented here (Fig. 6), show the same features as illustrated by Hesselbo *et al*. (2002, 2004) for St Audrie's Bay (SW England), Kuerschner *et al*. (2007) for the Tiefengraben section (Austria), Ward *et al*. (2007) for New York Canyon Ferguson Hill (Nevada, USA), and Williford *et al*. (2007) for Kennecott Point (Queen Charlotte Islands, British Columbia, Canada). The same major carbon-isotope fluctuations in the well-preserved marine oyster carbonate described here are also seen in bulk organic material (see Fig. 1), namely: (1) a sharp 'initial' negative excursion (here seen only in relatively low carbon isotope values at the base of the Langport Member), followed by (2) a 'boundary' positive excursion, and (3) an extended 'main' negative excursion.

It is noteworthy that the amplitudes of the carbon-isotope excursions are much larger (commonly twice the size) for the marine organic matter than for the carbonates, a common feature of carbon-isotope anomalies characterizing several Mesozoic–Cenozoic events (Arthur *et al*. 1988; Pagani *et al*. 2006; Hesselbo *et al*. 2007*a*). The general shape of the curve has been identified in other Triassic–Jurassic boundary sections for marine carbonates (e.g. McRoberts *et al*. 1997; Pálfy *et al*. 2001; Galli *et al*. 2005; van de Schootbrugge *et al*. 2007), but insufficient sampling density, lack of organic-matter-based records for the same strata, the occurrence of depositional hiatuses, or the effects of significant sediment redeposition, have made the identification of the negative–positive–negative geometry of the excursion in these sections uncertain.

The new data presented here demonstrate that the isotopic signature described is a seawater signal, and the similarity of the $\delta^{13}C$ records from carbonate and organic matter from different sections in the Tethyan and in North American regions strongly suggests that the carbon-isotope excursions are of global extent. Consequently, further definition of a high-resolution carbon-isotope stratigraphy has significant potential for improved correlation of a time interval beset with problems using only biostratigraphy.

In addition to insufficient sampling density and/or depositional hiatuses, diagenetic alteration must be considered when using the carbon-isotope curve for stratigraphic correlation. For the Langport Member and the lower Blue Lias Formation, carbon-isotope values from whole-rock carbonate at Lyme Regis show superficially the same $\delta^{13}C$ trend as oysters (Fig. 6), but the bulk-rock data are much more ^{13}C-depleted in the *planorbis*, *johnstoni* and *portlocki* subzones higher in the Blue Lias (about 2‰ lower than stratigraphically equivalent oysters). These isotopically lighter

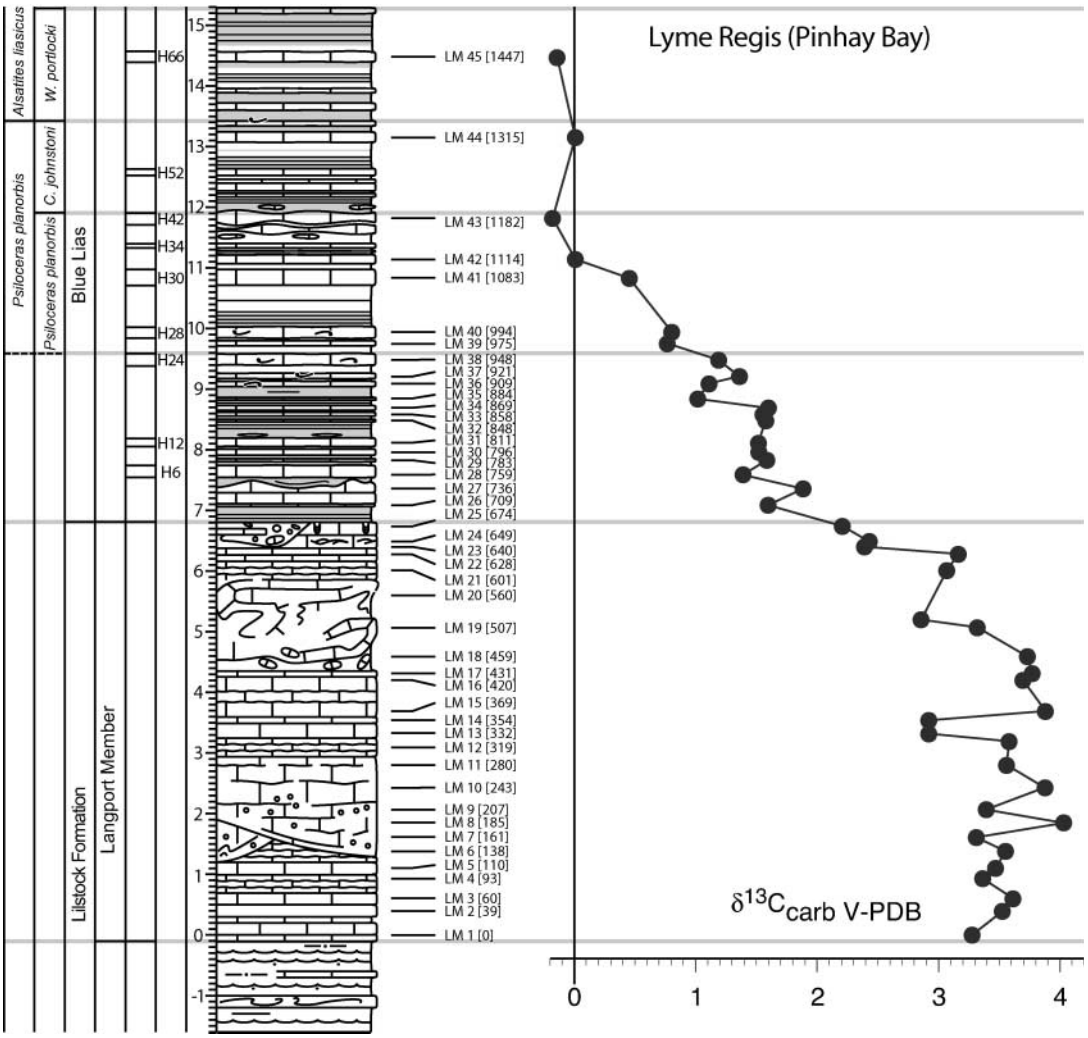

Fig. 5. Lithology and bulk $\delta^{13}C_{carb}$ data for the section at Pinhay Bay, Lyme Regis, SW England.

whole-rock $\delta^{13}C$ data are most probably diagenetically compromised because these carbonate beds are partly concretionary in origin, with ^{12}C-enriched carbon originating, at least in part (Fig. 8: dark grey field), from oxidized organic matter (Hallam 1960*b*; Weedon 1986; Sheppard *et al*. 2006). On the other hand, the data from the organic-lean Langport Member can be interpreted as more accurately representing the positive $\delta^{13}C$ excursion, and these relatively heavy values show that bulk-rock data, in this case deriving from massive micritic limestones, can preserve the primary seawater signature. Such carbonates were deposited as lime mud and peloids and lithified during diagenesis in an essentially closed system, such that the final $\delta^{13}C$ values of these limestones were probably derived from the dissolving solid phase of the original lime mud (see Veizer 1983). A correlation between Lyme Regis, St Audrie's Bay and Lavernock Point, based on carbon-isotopes, implies that the Langport Member at Lyme Regis is coeval with argillaceous facies in the Langport Member and Blue Lias at the other two localities (see Hesselbo *et al*. 2004).

Palaeoenvironmental change at the T–J boundary

The relationship between the T–J environmental crisis and flood-basalt volcanism of the Central Atlantic Magmatic Province (Fig. 1) has been much discussed, including the possibility that volcanogenic CO_2 was responsible for the negative carbon-isotope excursions (McHone 1996; Marzoli *et al*. 1999; Pálfy *et al*. 2000; Wignall 2001*b*; Courtillot & Renne 2003; Pálfy 2003; Nomade *et al*. 2007). Bulk-rock organic-carbon data from St Audrie's Bay show an abrupt 'initial' negative $\delta^{13}C$ excursion (Fig. 6). Such apparently sudden negative shifts could be accounted for by a local hiatus obscuring a more gradual change (see Hesselbo *et al*. 2002; Lucas *et al*. 2007), but the preponderance of records showing abrupt change (e.g. Hesselbo *et al*. 2002; Guex *et al*. 2004; Ward *et al*. 2007; Williford *et al*. 2007) implies either a relatively sudden event or an extraordinary synchroneity of sedimentary condensation.

Rather than being produced directly by volcanogenic CO_2 (see Self *et al*. 2006), such sudden negative carbon-isotope shifts are probably accounted for by the release of isotopically light carbon through other, less direct, mechanisms, such as those proposed for the Palaeocene–Eocene boundary and Toarcian Oceanic Anoxic Event: namely, massive methane release from gas hydrates (Dickens *et al*. 1995, 1997; Hesselbo *et al*. 2000; Kemp *et al*. 2005), and/or the intrusion of large sills into organic carbon-rich sedimentary strata (Svensen *et al*. 2004, 2007; McElwain *et al*. 2005).

In the case of the T–J boundary, intrusion of Central Atlantic

Table 3. *Whole-rock carbon- and oxygen-isotope data for the Pinhay Bay, Lyme Regis section*

Sample	Height above base of Langport Mbr (cm)	$\delta^{13}C$ (‰ V-PDB)	$\delta^{18}O$ (‰ V-PDB)
LM 1	0	3.28	−3.35
LM 2	39	3.53	−2.93
LM 3	60	3.61	−2.79
LM 4	93	3.36	−3.41
LM 5	110	3.47	−3.36
LM 6	138	3.55	−3.16
LM 7	161	3.31	−3.44
LM 8	185	4.03	−1.76
LM 9	207	3.39	−2.96
LM 10	243	3.88	−2.23
LM 11	280	3.56	−2.86
LM 12	319	3.58	−2.94
LM 13	332	2.92	−3.46
LM 14	354	2.92	−3.93
LM 15	369	3.88	−2.34
LM 16	420	3.70	−2.46
LM 17	431	3.77	−1.90
LM 18	459	3.73	−2.19
LM 19	507	3.32	−3.19
LM 20	520	2.86	−4.56
LM 21	601	3.07	−2.92
LM 22	628	3.16	−2.86
LM 23	640	2.39	−3.14
LM 24	649	2.43	−2.81
LM 25	674	2.21	−3.04
LM 26	709	1.60	−4.58
LM 27	736	1.89	−2.90
LM 28	759	1.39	−2.08
LM 29	783	1.59	−2.17
LM 30	796	1.52	−1.98
LM 31	811	1.52	−2.86
LM 32	848	1.58	−3.16
LM 33	858	1.55	−3.09
LM 34	869	1.60	−2.79
LM 35	884	1.02	−3.93
LM 36	909	1.11	−3.09
LM 37	921	1.36	−2.30
LM 38	948	1.19	−2.23
LM 39	975	0.77	−2.36
LM 40	994	0.80	−2.32
LM 41	1083	0.45	−1.53
LM 42	1114	0.01	−2.62
LM 43	1182	-0.18	−1.90
LM 44	1315	0.01	−2.12
LM 45	1447	-0.14	−1.89

Isotope laboratory: Oxford.

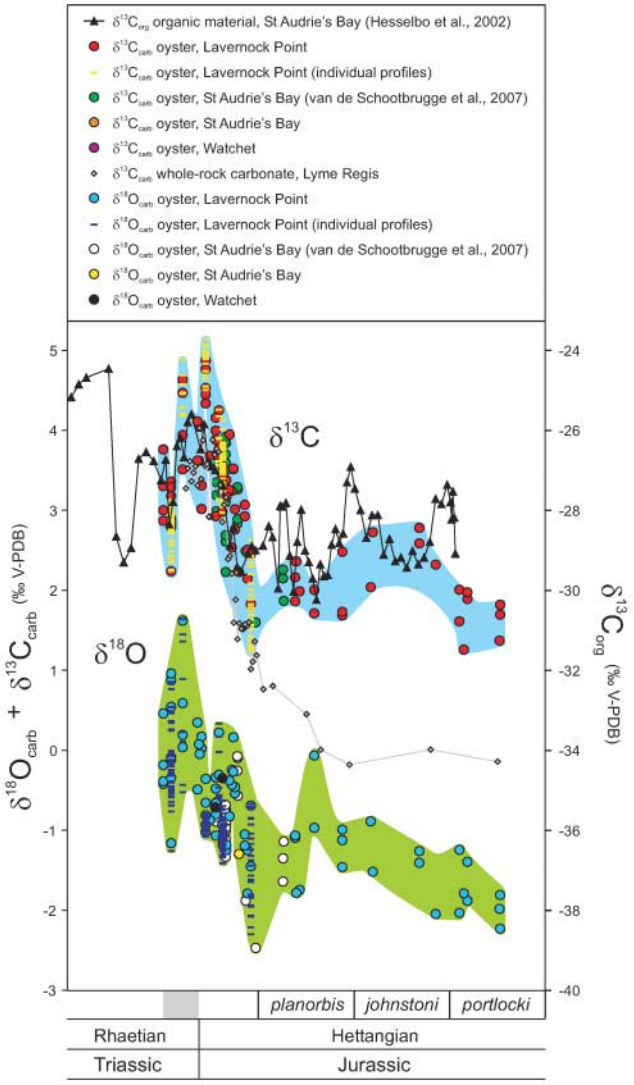

Fig. 6. $\delta^{13}C$ and $\delta^{18}O$ values for all well-preserved oysters for the Triassic–Jurassic transition from Lavernock Point, Watchet and St Audrie's Bay (including data from van de Schootbrugge *et al*. 2007), and carbon-isotope data from whole-rock carbonates from Lyme Regis. Bulk organic $\delta^{13}C$ data (Hesselbo *et al*. 2002, 2004) are also plotted for comparison. Correlations between St Audrie's Bay, Watchet and Lavernock are based on lithostratigraphy and biostratigraphy. Correlation between Lyme Regis and the other localities is based upon biostratigraphy for the Blue Lias and carbon-isotope data for the Langport Member. Ages are assigned to the data points based on the position of samples at each locality within the recognized ammonite subzones (see Jenkyns *et al*. 2002), with the addition of a notional subzone to span the gap between the base of the *planorbis* Subzone and the proposed (lower) base of the Hettangian. Data points in the Triassic are plotted assuming a constant sedimentation rate through the earliest Jurassic at Lavernock Point and St Audrie's Bay.

Magmatic Province magma into organic-rich lacustrine sediments of the deep and extensive Triassic rift systems could have caused similar effects. A large proportion of the Central Atlantic Magmatic Province intrusive bodies are either eroded or deeply buried beneath later Mesozoic deposits on the continental margins (McHone 1996) and the nature of the material into which the magma was intruded is generally unknown. In the Newark Basin, one of these Triassic rift basins, dolerite sills are locally intruded into Carnian lacustrine black shales of the Lockatong Formation, which have undergone intense thermal metamorphism (Van Houten 1969, 1971). Thus, although the extent to which this may have been an effective process in generation of isotopically light thermogenic methane is uncertain, it is known that such processes occurred on at least a local scale during T–J boundary time.

Positive carbon-isotope excursions are usually explained by accelerated burial of organic carbon (Scholle & Arthur 1980; Kump & Arthur 1999). For the pronounced earliest Jurassic positive excursion (Fig. 6), an origin through globally accelerated carbon burial cannot at present be demonstrated, largely because the stratigraphic record for this time interval is so fragmentary. At St Audrie's Bay, although the equivalent strata are not

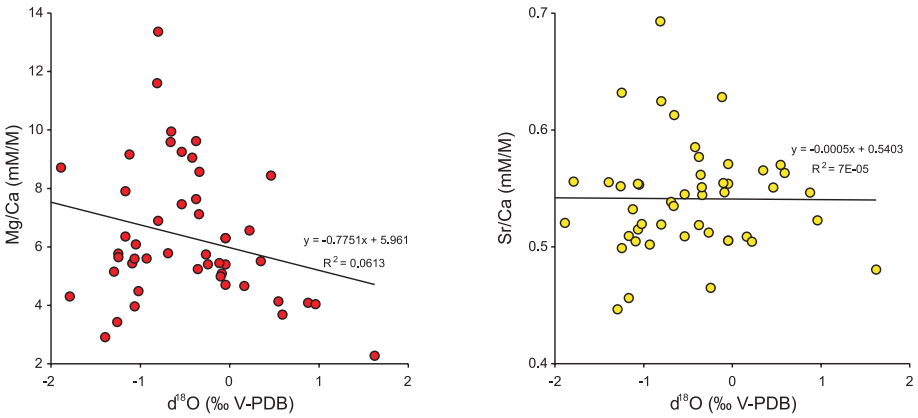

Fig. 7. Cross-plots for $\delta^{18}O$ against Mg/Ca and Sr/Ca.

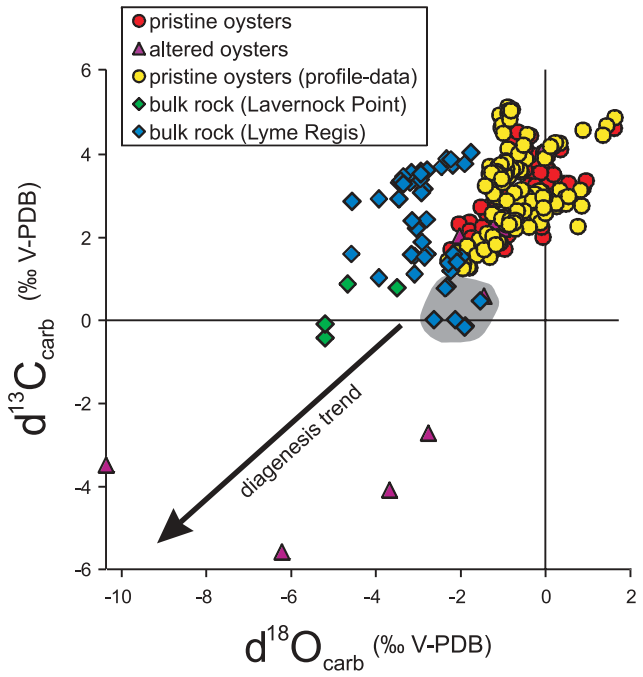

Fig. 8. Cross-plot for $\delta^{13}C$ against $\delta^{18}O$ values of all pristine and altered oysters (Lavernock Point, Watchet and St Audrie's Bay) as well as bulk-rock samples (Lyme Regis and Lavernock Point). It should be noted that altered oysters as well as bulk-rock samples tend to show lower $\delta^{18}O$ and partly also lower $\delta^{13}C$ values than unaltered oysters.

markedly enriched in organic carbon, they are strongly laminated (Hesselbo *et al*. 2004), indicating bottom-water anoxia and the potential for enhanced organic matter burial at other localities.

Oxygen-isotope values in the calcitic shells of oysters are controlled by the seawater $\delta^{18}O$, pH and temperature (Zeebe & Wolf-Gladrow 2001). Assuming that seawater pH was similar to the present-day value and seawater $\delta^{18}O$ was about −1.2‰ in an ice-free world (Zachos *et al*. 2001), bottom-water temperatures, using the equation of O'Neil *et al*. (1969), were between <7 and 14 °C for deposition of the upper Langport Member and between *c*. 12 and 22 °C for the *planorbis*, *johnstoni* and *portlocki* ammonite Subzones. Assuming no change in the local seawater $\delta^{18}O$ over the interval in question, these data indicate a temperature increase of more than 8 °C for the bottom waters in the vicinity of the Lavernock Point locality. Starting from relatively cool initial temperatures, a warming occurred in concert with the shift towards negative carbon-isotope values.

It might be argued that the decreasing oxygen-isotope trend that occurs leading into the *planorbis* Zone was caused, at least in part, by a lowering of the local or global seawater $\delta^{18}O$ rather than a rise in temperature. Changes in global seawater $\delta^{18}O$ related to interaction of seawater with the lithosphere are on multi-million year time scales (Gregory 1991; Veizer *et al*. 1999) and can be excluded as an explanation. Short-term lowering of the seawater $\delta^{18}O$ could be caused by melting of continental ice, in the manner observed for the post-Eocene 'icehouse' (Shackleton & Opdyke 1973). The extent of continental ice during supposed 'greenhouse' times is a matter of much speculation and few data (Price 1999; Miller *et al*. 2005). Climate modelling studies that have been carried out for the T–J boundary interval have been aimed at testing the environmental response of the T–J world to increased rather than decreased atmospheric CO_2 partial pressures; nevertheless, polar regions of the Earth experience polar ice-forming conditions in simulations with 2 × pre-industrial atmospheric CO_2 content (Huynh & Poulsen 2005). It is notable, however, that the lightening in oxygen-isotope values observed in the present study would have corresponded to a eustatic sea-level rise of some 200 m if generated by waning ice sheets (see Miller *et al*. 2005) and, although a sea-level rise is compatible with sequence stratigraphic interpretations for this time interval, the large magnitude is not (Hesselbo 2008, and references therein).

Lastly, a localized change in salinity may be postulated, either from normal marine to freshwater conditions, or from hypersaline to normal marine conditions. An upward trend towards greater freshwater influence is implausible because ammonites appear at the culmination of the trend to lighter isotope values, the exact opposite of what would be expected. An upward trend from hypersaline to normal marine waters can also be ruled out because Jurassic oysters and their modern counterparts are intolerant of hypersaline conditions, occupying brackish to normal marine habitats (Hendry & Kalin 1997; Fürsich 1993). In an isotopic study of Middle Jurassic oysters from England, Hendry & Kalin (1997) explained heavy oxygen isotopes in shells from nearshore settings as a result of evaporative concentration within low-salinity waters of hydrodynamically closed lagoons, a palaeogeographical setting that is very different from the one considered here.

Faunal evidence, particularly the occurrence of corals, echinoderms and conodonts, led Swift (1995) and Swift and Martill (1999) to argue in favour of a normal marine environment for the Langport Member in southern Britain. The absence of other

typically normal marine taxa such as brachiopods and ammonites may be due to the severe ecological disturbance that occurred during the Triassic–Jurassic boundary mass extinction rather than simple salinity control. Celestine in the Langport Member of Devon was interpreted by Hesselbo & Jenkyns (1995) as a possible replacement of evaporitic gypsum. However, this observation is of only marginal relevance to interpretation of the Lavernock oyster oxygen-isotope data, which come from a different facies and a distant location.

With regard to a detailed comparison between the carbon-isotope and oxygen-isotope curves presented in this study, a small difference in the position of the positive peaks is detected, with the peak in oxygen-isotope values occurring a few decimetres lower in the section than the peak in carbon-isotope values. However, these differences may reasonably be regarded as a consequence of the variability exhibited within single shells and between shells taken from the same horizon. The data do not clearly define a phase lag between the oxygen- and carbon-isotope curves.

The relationship between palaeotemperature change (as inferred from oxygen-isotope values) and carbon-isotope fluctuations is similar to that observed for the Toarcian Oceanic Anoxic Event (Hesselbo *et al*. 2007*b*), during which high temperatures coincided with strongly negative carbon-isotope values, and lower temperatures with more positive carbon-isotope values (and enhanced organic-carbon burial causing drawdown of atmospheric CO_2). The T–J boundary results are compatible with the interpretation that positive carbon-isotope excursions correspond to times of low atmospheric carbon dioxide content, and negative carbon-isotope excursions correspond to times of high atmospheric carbon dioxide content, implying significant swings in the balance between carbon drawdown through organic-matter burial and recycling of isotopically light carbon from endogenic or exogenic sources.

Conclusions

Major carbon-isotope fluctuations are preserved within low-Mg calcite shells of oysters collected at T–J boundary sections in SW Britain. These fluctuations follow trends previously established from bulk organic-matter samples from the same sedimentary basin, and thus confirm that the observed isotopic signals capture characteristics of the local water masses. Furthermore, the similarity to carbon-isotope curves generated from other basins suggests that the signal is global. The amplitude of the carbonate carbon-isotope fluctuations is about half that observed from organic matter, a feature common to other Mesozoic and Early Cenozoic events affecting the global carbon cycle. The T–J boundary isotopic excursions occurred coincident with Central Atlantic Magmatic Province continental flood-basalt volcanism, and may have been triggered by the intrusion of mantle-derived melts into carbon-rich sedimentary deposits and/or dissociation of gas hydrates triggered by a global rise in temperature. The pronounced positive carbon-isotope anomaly is associated with relatively heavy seawater oxygen-isotope values, indicating cool conditions, possibly associated with enhanced organic-carbon burial and drawdown of atmospheric carbon dioxide. The subsequent trend towards lighter seawater oxygen-isotope values indicates returning warmer temperatures that parallel a return to lighter carbon-isotope values and inferred build-up of atmospheric carbon dioxide. Mg/Ca and Sr/Ca ratios show no significant correlation to $\delta^{18}O$, indicating that Mg and Sr incorporation in the investigated *Liostrea hisingeri* is controlled mainly by factors other than temperature.

We acknowledge P. Hodges (Cardiff) for scientific discussion in the field, and N. Charnley, J. Arden, C.-J. de Hoog (all Oxford), U. Schulte, W. Gosda (both Bochum) and M. Wimmer (Innsbruck) for stable-isotope and elemental analyses. We thank the Deutsche Akademie der Naturforscher Leopoldina (BMBF-LPD 9901/8-116) for contributions to the financing of this project. P. Olsen is thanked for scientific discussion. Finally, we thank J. Pálfy, I. Jarvis and an anonymous referee for their insightful critical comments.

References

Andrus, C.F.T. & Crowe, D.E. 2000. Geochemical analysis of *Crassostrea virginica* as a method to determine season of capture. *Journal of Archaeological Science*, **27**, 33–42.

Arthur, M.A., Dean, W.E. & Pratt, L.M. 1988. Geochemical and climatic effects of increased marine organic carbon burial at the Cenomanian/Turonian boundary. *Nature*, **335**, 714–717.

Boyle, E.A. & Keigwin, L.D. 1985. Comparison of Atlantic and Pacific paleochemical records for the last 215,000 years: changes in deep ocean circulation and chemical inventories. *Earth and Planetary Science Letters*, **76**, 135–150.

Brand, U. & Veizer, J. 1980. Chemical diagenesis of a multicomponent carbonate system—1: Trace elements. *Journal of Sedimentary Petrology*, **50**, 1219–1236.

Carter, J.G. 1990. Evolutionary significance of shell microstructure in the Palaeotaxodonta, Pteriomorphia and Isofilibranchia. *In:* Carter, J.G. (ed.) *Skeletal Biomineralization, Patterns, Processes and Evolutionary Trends*. Van Nostrand Reinhold, New York, 135–412.

Cohen, A.S. & Coe, A.L. 2002. New geochemical evidence for the onset of volcanism in the Central Atlantic magmatic province and environmental change at the Triassic–Jurassic boundary. *Geology*, **30**, 267–270.

Cohen, A.S. & Coe, A.L. 2007. The impact of the Central Atlantic Magmatic Province on climate and on the Sr- and Os-isotope evolution of seawater. *Palaeogeography, Palaeoclimatology, Palaeoecology*, **244**, 374–390.

Courtillot, V.E. & Renne, P.R. 2003. On the ages of flood basalt events. *Comptes Rendus Géoscience*, **335**, 113–140.

Dickens, G.R., O'Neil, J.R., Rea, D.K. & Owen, R.M. 1995. Dissociation of oceanic methane hydrate as a cause of the carbon isotope excursion at the end of the Paleocene. *Paleoceanography*, **10**, 965–971.

Dickens, G.R., Castillo, M.M. & Walker, J.C.G. 1997. A blast of gas in the latest Paleocene: simulating first-order effects of massive dissociation of oceanic methane hydrate. *Geology*, **25**, 259–262.

Dodd, J.R. 1965. Environmental control of strontium and magnesium in *Mytilus*. *Geochimica et Cosmochimica Acta*, **29**, 385–398.

Freitas, P.S., Clarke, L.J., Kennedy, H., Richardson, C.A. & Abrantes, F. 2006. Environmental and biological controls on elemental (Mg/Ca, Sr/Ca and Mn/Ca) ratios in shells of the king scallop *Pecten maximus*. *Geochimica et Cosmochimica Acta*, **70**, 5119–5133.

Fürsich, F.T. 1993. Palaeoecology and evolution of Mesozoic salinity-controlled benthic macroinvertebrate associations. *Lethaia*, **26**, 327–346.

Galli, M.T., Jadoul, F., Bernasconi, S.M. & Weissert, H. 2005. Anomalies in global carbon cycling and extinction at the Triassic/Jurassic boundary: evidence from a marine C-isotope record. *Palaeogeography, Palaeoclimatology, Palaeoecology*, **216**, 203–214.

Galli, M.T., Jadoul, F., Bernasconi, S.M., Cirilli, S., Weissert, H. 2007. Stratigraphy and palaeoenvironmental analysis of the Triassic–Jurassic transition in the western Southern Alps (Northern Italy). *Palaeogeography, Palaeoclimatology, Palaeoecology*, **244**, 52–70.

Gregory, R.T. 1991. Oxygen isotope history of seawater revisited: Timescales for boundary event changes in the oxygen isotope composition of seawater. *In:* Taylor, H.P., O'Neil, J.R. & Kaplan, I.R. (eds) *Stable Isotope Geochemistry: A Tribute to Samuel Epstein*. Geochemical Society Special Publications, **3**, 65–76.

Guex, J., Bartolini, A., Atudorei, V. & Taylor, D. 2004. High-resolution ammonite and carbon isotope stratigraphy across the Triassic–Jurassic boundary at New York Canyon (Nevada). *Earth and Planetary Science Letters*, **225**, 29–41.

Hallam, A. 1960*a*. The White Lias of the Devon coast. *Proceedings of the Geologists' Association*, **71**, 47–60.

Hallam, A. 1960*b*. A sedimentary and faunal study of the Blue Lias of Dorset and Glamorgan. *Philosophical Transactions of the Royal Society of London, Series B*, **243**, 1–44.

Hallam, A. & Wignall, P.B. 1997. *Mass Extinctions and their Aftermath*. Oxford University Press, Oxford.

Hansen, H.J. 2006. Stable isotopes of carbon from basaltic rocks and their possible relation to atmospheric isotope excursions. *Lithos*, **92**, 105–116.

Harding, D.J., Arden, J.W. & Rickaby, R.E.M. 2006. A method for precise analysis of trace element/calcium ratios in carbonate samples using quadrupole inductively coupled plasma mass spectrometry. *Geochemistry, Geophysics, Geosystems*, **7**, Q06003, doi:10.1029/2005GC001093.

Hautmann, M. 2006. Shell mineralogical trends in epifaunal Mesozoic bivalves and their relationship to seawater chemistry and atmospheric carbon dioxide concentration. *Facies*, **52**, 417–433.

Hayes, J.M., Strauss, H. & Kaufman, A.J. 1999. The abundance of ^{13}C in marine organic matter and isotopic fractionation in the global biogeochemical cycle of carbon during the past 800 Ma. *Chemical Geology*, **161**, 103–125.

Hendry, J.P. & Kalin, R.M. 1997. Are oxygen and carbon isotopes of mollusc shells reliable palaeosalinity indicators in marginal marine environments? A case study from the Middle Jurassic of England. *Journal of the Geological Society, London*, **154**, 321–333.

Hesselbo, S.P. 2008. Sequence stratigraphy and inferred relative sea-level change from the onshore British Jurassic. *Proceedings of the Geologists' Association*, **119**, 19–34.

Hesselbo, S.P. & Jenkyns, H.C. 1995. A comparison of the Hettangian to Bajocian successions of Dorset and Yorkshire. *In:* Taylor, P.D. (ed.) *Field Geology of the British Jurassic*. Geological Society, London, 105–150.

Hesselbo, S.P., Gröcke, D.R., Jenkyns, H.C., Bjerrum, C.J., Farrimond, P., Morgans Bell, H.S. & Green, O.R. 2000. Massive dissociation of gas hydrate during a Jurassic Oceanic Anoxic Event. *Nature*, **406**, 392–395.

Hesselbo, S.P., Robinson, S.A., Surlyk, F. & Piasecki, S. 2002. Terrestrial and marine extinction at the Triassic–Jurassic boundary synchronized with major carbon-cycle perturbation: A link to initiation of massive volcanism? *Geology*, **30**, 251–254.

Hesselbo, S.P., Robinson, S.A. & Surlyk, F. 2004. Sea-level change and facies development across potential Triassic–Jurassic boundary horizons, SW Britain. *Journal of the Geological Society, London*, **161**, 365–379.

Hesselbo, S.P., McRoberts, C.A. & Pálfy, J. 2007*a*. Triassic–Jurassic boundary events: problems, progress, possibilities. *Palaeogeography, Palaeoclimatology, Palaeoecology*, **244**, 1–10.

Hesselbo, S.P., Jenkyns, H.C., Duarte, L.V. & Oliveira, L.C.V. 2007*b*. Carbon-isotope record of the Early Jurassic (Toarcian) Oceanic Anoxic Event from fossil wood and marine carbonate (Lusitanian Basin, Portugal). *Earth and Planetary Science Letters*, **253**, 455–470.

Hodges, P. 1994. The base of the Jurassic system: new data on the first appearance of *Psiloceras planorbis* in southwest England. *Geological Magazine*, **131**, 841–844.

Hounslow, M.W., Posen, P.E. & Warrington, G. 2004. Magnetostratigraphy and biostratigraphy of the Upper Triassic and lowermost Jurassic succession, St Audrie's Bay, UK. *Palaeogeography, Palaeoclimatology, Palaeoecology*, **213**, 331–358.

Hubbard, R.N.L.B. & Boulter, M.C. 2000. Phytogeography and paleoecology in Western Europe and Eastern Greenland near the Triassic–Jurassic boundary. *Palaios*, **15**, 120–131.

Huynh, T.T. & Poulsen, C.J. 2005. Rising atmospheric CO_2 as a possible trigger for the end-Triassic mass extinction. *Palaeogeography, Palaeoclimatology, Palaeoecology*, **217**, 223–242.

Jarvis, I., Gale, A.S., Jenkyns, H.C. & Pearce, M.A. 2006. Secular variation in Late Cretaceous carbon isotopes: a new $\delta^{13}C$ carbonate reference curve for the Cenomanian–Campanian (99.6–70.6 Ma). *Geological Magazine*, **143**, 561–608.

Jenkyns, H.C. 1996. Relative sea-level change and carbon isotopes: data from the Upper Jurassic (Oxfordian) of central and Southern Europe. *Terra Nova*, **8**, 75–85.

Jenkyns, H.C. 2003. Evidence for rapid climate change in the Mesozoic–Palaeogene greenhouse world. *Philosophical Transactions of the Royal Society of London, Series A*, **361**, 1885–1916.

Jenkyns, H.C., Jones, C.E., Gröcke, D.R., Hesselbo, S.P. & Parkinson, D.N. 2002. Chemostratigraphy of the Jurassic System: applications, limitations and implications for palaeoceanography. *Journal of the Geological Society, London*, **159**, 351–378.

Kemp, D.B., Coe, A.L., Cohen, A.S. & Schwark, L. 2005. Astronomical pacing of methane release in the Early Jurassic period. *Nature*, **437**, 396–399.

Kiessling, W., Aberhan, M., Brenneis, B. & Wagner, P.J. 2007. Extinction trajectories of benthic organisms across the Triassic–Jurassic boundary. *Palaeogeography, Palaeoclimatology, Palaeoecology*, **244**, 201–222.

Kirby, M.X. 2000. Paleoecological differences between Tertiary and Quaternary *Crassostrea* oysters, as revealed by stable isotope sclerochronology. *Palaios*, **15**, 132–141.

Kirby, M.X., Soniat, T.M. & Spero, H.J. 1998. Stable isotope sclerochronology of Pleistocene and Recent oyster shells (*Crassostrea virginica*). *Palaios*, **13**, 560–569.

Klein, R.T., Lohmann, K.C. & Thayer, C.W. 1996*a*. Bivalve skeletons record sea-surface temperature and $\delta^{18}O$ via Mg/Ca and $^{18}O/^{16}O$ ratios. *Geology*, **24**, 415–418.

Klein, R.T., Lohmann, K.C. & Thayer, C.W. 1996*b*. Sr/Ca and $^{13}C/^{12}C$ ratios in skeletal calcite of *Mytilus trossulus*: Covariation with metabolic rate, salinity, and carbon isotopic composition of seawater. *Geochimica et Cosmochimica Acta*, **60**, 4207–4221.

Knoll, A.H., Bambach, R.K., Canfield, D.E. & Grotzinger, J.P. 1996. Comparative Earth history and late Permian mass extinction. *Science*, **273**, 452–457.

Korte, C. & Kozur, H.W. 2005. Carbon isotope stratigraphy across the Permian/Triassic boundary at Jolfa (NW-Iran), Peitlerkofel (Sas de Pütia, Sass de Putia), Pufels (Bula, Bulla), Tesero (all three Southern Alps, Italy) and Gerennavár (Bükk Mts., Hungary). *Journal of Alpine Geology*, **47**, 119–135.

Korte, C., Kozur, H.W., Bruckschen, P. & Veizer, J. 2003. Strontium isotope evolution of Late Permian and Triassic seawater. *Geochimica et Cosmochimica Acta*, **67**, 47–62.

Korte, C., Jasper, T., Kozur, H.W. & Veizer, J. 2005*a*. $\delta^{18}O$ and $\delta^{13}C$ of Permian brachiopods: A record of seawater evolution and continental glaciation. *Palaeogeography, Palaeoclimatology, Palaeoecology*, **224**, 333–351.

Korte, C., Kozur, H.W. & Veizer, J. 2005*b*. $\delta^{13}C$ and $\delta^{18}O$ values of Triassic brachiopods and carbonate rocks as proxies for coeval seawater and palaeotemperature. *Palaeogeography, Palaeoclimatology, Palaeoecology*, **226**, 287–306.

Korte, C., Jasper, T., Kozur, H.W. & Veizer, J. 2006. $^{87}Sr/^{86}Sr$ record of Permian seawater. *Palaeogeography, Palaeoclimatology, Palaeoecology*, **240**, 89–107.

Korte, C., Jones, P.J., Brand, U., Mertmann, D. & Veizer, J. 2008. Oxygen isotope values from high latitudes: Clues for Permian sea-surface temperature gradients and Late Palaeozoic deglaciation. *Palaeogeography, Palaeoclimatology, Palaeoecology*, **269**, 1–16.

Kuerschner, W.M., Bonis, N.R. & Krystyn, L. 2007. Carbon-isotope stratigraphy and palynostratigraphy of the Triassic–Jurassic transition in the Tiefengraben section—Northern Calcareous Alps (Austria). *Palaeogeography, Palaeoclimatology, Palaeoecology*, **244**, 257–280.

Kump, L.R. & Arthur, M.A. 1999. Interpreting carbon-isotope excursions: Carbonates and organic matter. *Chemical Geology*, **161**, 181–198.

Küspert, W. 1982. Environmental changes during oil shale deposition as deduced from stable isotope ratios. *In:* Einsele, G. & Seilacher, A. (eds) *Cyclic and Event Stratification*. Springer, Berlin, 482–501.

Lang, W.D. 1924. The Blue Lias of the Devon and Dorset coasts. *Proceedings of the Geologists' Association*, **35**, 169–185.

Lorrain, A., Gillikin, D.P., Paulet, Y.-M., Chauvaud, L., Le Mercier, A., Navez, J. & André,L. 2005. Strong kinetic effects on Sr/Ca ratios in the calcitic bivalve *Pecten maximus*. *Geology*, **33**, 965–968.

Lowenstam, H.A. & Weiner, S. 1989. *On Biomineralization. Mollusca*. Oxford University Press, Oxford, 88–134.

Lucas, S.G., Taylor, D.G., Guex, J., Tanner, L.H. & Krainer, K. 2007. The proposed global stratotype section and point for the base of the Jurassic System in the New York Canyon area, Nevada, USA. *In:* Lucas, S.G. & Spielmann, J.A. (eds) *Triassic of the American West*. New Mexico Museum of Natural History and Science, Bulletin, **40**, 139–168.

Marzoli, A., Renne, P.R., Piccirillo, E.M., Ernesto, M., Bellieni, G. & De Min, A. 1999. Extensive 200-million-year-old continental flood basalts of the central Atlantic magmatic province. *Science*, **284**, 616–618.

McElwain, J.C., Beerling, D.J. & Woodward, F.I. 1999. Fossil plants and global warming at the Triassic–Jurassic boundary. *Science*, **285**, 1386–1390.

McElwain, J.C., Murphy, J.W. & Hesselbo, S.P. 2005. Changes in carbon dioxide during an oceanic anoxic event linked to intrusion of Gondwana coals. *Nature*, **435**, 479–483.

McHone, J.G. 1996. Broad-terrane Jurassic flood basalts across northeastern North America. *Geology*, **24**, 319–322.

McHone, J.G. 2000. Non-plume magmatism and rifting during the opening of the central Atlantic Ocean. *Tectonophysics*, **316**, 287–296.

McRoberts, C.A., Furrer, H. & Jones, D.S. 1997. Palaeoenvironmental interpretation of a Triassic–Jurassic boundary section from Western Austria based on palaeoecological and geochemical data. *Palaeogeography, Palaeoclimatology, Palaeoecology*, **136**, 79–95.

McRoberts, C.A., Ward, P.D. & Hesselbo, S.P. 2007. A proposal for the base Hettangian Stage (= base Jurassic System) GSSP at New York Canyon (Nevada, USA) using carbon isotopes. *International Subcommission on Jurassic Stratigraphy Newsletter*, **34**, 43–49.

Miller, K.G., Wright, J.D. & Browning, J.V. 2005. Visions of ice sheets in a greenhouse world. *Marine Geology*, **217**, 215–231.

Mount, A.S., Wheeler, A.P., Paradkar, R.P. & Snider, D. 2004. Hemocyte-mediated shell mineralization in the eastern oyster. *Science*, **304**, 297–300.

Nomade, S., Knight, K.B., Beutel, E., *et al.* 2007. Chronology of the Central Atlantic Magmatic Province: Implications for the Central Atlantic rifting processes and the Triassic–Jurassic biotic crisis. *Palaeogeography, Palaeoclimatology, Palaeoecology*, **244**, 326–344.

O'Neil, J.R., Clayton, R.N. & Mayeda, T.K. 1969. Oxygen isotope fractionation in divalent metal carbonates. *Journal of Chemical Physics*, **51**, 5547–5558.

Pagani, M., Pedentchouk, N., Huber, M., *et al.* 2006. Arctic hydrology during global warming at the Palaeocene/Eocene thermal maximum. *Nature*, **442**, 671–675.

Pálfy, J. 2003. Volcanism of the Central Atlantic Magmatic Province as a potential driving force in the end-Triassic mass extinction. *In:* Hames, W.E., McHone, J.G., Renne, P. & Ruppel, C. (eds) *The Central Atlantic Magmatic Province: Insights from fragments of Pangea*. American Geophysical Union, Geophysical Monograph Series, **136**, 255–267.

Pálfy, J., Mortensen, J.K., Carter, E.S., Smith, P.L., Friedman, R.M. & Tipper, H.W. 2000. Timing of the end-Triassic mass extinction: First on land, then in the sea? *Geology*, **28**, 39–42.

Pálfy, J., Demény, A., Haas, J., Hetényi, M., Orchard, M.J. & Vető, I. 2001. Carbon isotope anomaly and other geochemical changes at the Triassic–Jurassic boundary from a marine section in Hungary. *Geology*, **29**, 1047–1050.

Pálfy, J., Demény, A., Haas, J., *et al.* 2007. Triassic–Jurassic boundary events inferred from integrated stratigraphy of the Csővár section, Hungary. *Palaeogeography, Palaeoclimatology, Palaeoecology*, **244**, 11–33.

Price, G.D. 1999. The evidence and implications of polar ice during the Mesozoic. *Earth-Science Reviews*, **48**, 183–210.

Richardson, L. 1905. The Rhaetic and contiguous deposits of Glamorganshire. *Quarterly Journal of the Geological Society of London*, **61**, 385–424.

Richardson, L. 1906. On the Rhaetic and contiguous deposits of Devon and Dorset. *Proceedings of the Geologists' Association*, **14**, 401–409.

Richardson, L. 1911. The Rhaetic and contiguous deposits of West, Mid, and part of East Somerset. *Quarterly Journal of the Geological Society of London*, **67**, 1–74.

Rickaby, R.E.M. & Halloran, P. 2005. Cool La Niña during the warmth of the Pliocene? *Science*, **307**, 1948–1952.

Rosenthal, Y., Field, M.P. & Sherrell, R.M. 1999. Precise determination of element/calcium ratios in calcareous samples using sector field inductively coupled plasma mass spectrometry. *Analytical Chemistry*, **71**, 3248–3253.

Scholle, P.A. & Arthur, M.A. 1980. Carbon isotope fluctuations in Cretaceous pelagic limestones: potential stratigraphic and petroleum exploration tool. *AAPG Bulletin*, **64**, 67–87.

Shackleton, N.J. & Opdyke, N.D. 1973. Oxygen isotope and palaeomagnetic stratigraphy of equatorial Pacific core V28-238: Oxygen isotope temperatures and ice volumes on a 10^5 year and 10^6 year scale. *Quaternary Research*, **3**, 39–55.

Sheppard, T.H., Houghton, R.D. & Swan, A.R.H. 2006. Bedding and pseudobedding in the Early Jurassic of Glamorgan: deposition and diagenesis of the Blue Lias in South Wales. *Proceedings of the Geologists' Association*, **117**, 249–264.

Self, S., Widdowson, M., Thordarson, T. & Jay, A.E. 2006. Volatile fluxes during flood basalt eruptions and potential effects on the global environment: A Deccan perspective. *Earth and Planetary Science Letters*, **248**, 518–532.

Spötl, C. & Vennemann, T.W. 2003. Continuous-flow isotope ratio mass spectrometric analysis of carbonate minerals. *Rapid Communications in Mass Spectrometry*, **17**, 1004–1006.

Stecher, H.A., Krantz, D.E., Lord, C.J., Luther, G.W. & Bock, K.W. 1996. Profiles of strontium and barium in *Mercenaria mercenaria* and *Spisula solidissima* shells. *Geochimica et Cosmochimica Acta*, **60**, 3445–3456.

Steuber, T. & Veizer, J. 2002. Phanerozoic record of plate tectonic control of seawater chemistry and carbonate sedimentation. *Geology*, **30**, 1123–1126.

Surge, D., Lohmann, K.C. & Dettman, D.L. 2001. Controls on isotopic chemistry of the American oyster, *Crassostrea virginica*: implications for growth patterns. *Palaeogeography, Palaeoclimatology, Palaeoecology*, **172**, 283–296.

Svensen, H., Planke, S., Malthe-Sørenssen, A., Jamtveit, B., Myklebust, R., Eidem, T.R. & Rey, S.S. 2004. Release of methane from a volcanic basin as a mechanism for initial Eocene global warming. *Nature*, **429**, 542–545.

Svensen, H., Planke, S., Chevallier, L., Malthe-Sørenssen, A., Corfu, F. & Jamtveit, B. 2007. Hydrothermal venting of greenhouse gases triggering Early Jurassic global warming. *Earth and Planetary Science Letters*, **256**, 554–566.

Swift, A. 1995. A review of the nature and outcrop of the 'White Lias' facies of the Langport Member (Penarth Group: Upper Triassic) in Britain. *Proceedings of the Geologists' Association*, **106**, 247–258.

Swift, A. & Martill, D.M. 1999. *Fossils of the Rhaetian Penarth Group*. Blackwell for the Palaeontological Association, London.

Tomašových, A. & Siblík, M. 2007. Evaluating compositional turnover of brachiopod communities during the end-Triassic mass extinction (Northern Calcareous Alps): Removal of dominant groups, recovery and community reassembly. *Palaeogeography, Palaeoclimatology, Palaeoecology*, **244**, 170–200.

Trueman, A.E. 1920. The Liassic rocks of the Cardiff district. *Proceedings of the Geologists' Association*, **31**, 93–107.

vander Putten, E., Dehairs, F., Keppens, E. & Baeyens, W. 2000. High resolution distribution of trace elements in the calcite shell layer of modern *Mytilus edulis*: environmental and biological controls. *Geochimica et Cosmochimica Acta*, **64**, 997–1011.

van de Schootbrugge, B., Tremolada, F., Rosenthal, Y., *et al.* 2007. End-Triassic calcification crisis and blooms of organic-walled 'disaster species'. *Palaeogeography, Palaeoclimatology, Palaeoecology*, **244**, 126–141.

Van Houten, F.B. 1969. Late Triassic Newark Group, north-central New Jersey and adjacent New York and Pennsylvania. *In:* Subitzky, S. (ed.) *Geology of Selected Areas in New Jersey and Pennsylvania*. Geological Society of America and Rutgers University Press, New Brunswick, NJ, 314–348.

Van Houten, F.B. 1971. Contact metamorphic mineral assemblages, Late Triassic Newark Group, New Jersey. *Contributions to Mineralogy and Petrology*, **30**, 1–14.

Veizer, J. 1983. Trace elements and isotopes in sedimentary carbonates. *In:* Reeder, R.J. (ed.) *Carbonates: Mineralogy and Chemistry*. Mineralogical Society of America, Reviews in Mineralogy, **11**, 265–299.

Veizer, J., Bruckschen, P., Pawellek, F., *et al.* 1997*a*. Oxygen isotope evolution of Phanerozoic seawater. *Palaeogeography, Palaeoclimatology, Palaeoecology*, **132**, 159–172.

Veizer, J., Buhl, D., Diener, A., *et al.* 1997*b*. Strontium isotope stratigraphy: potential resolution and event correlation. *Palaeogeography, Palaeoclimatology, Palaeoecology*, **132**, 65–77.

Veizer, J., Ala, D., Azmy, K., *et al.* 1999. $^{87}Sr/^{86}Sr$, $\delta^{13}C$ and $\delta^{18}O$ evolution of Phanerozoic seawater. *Chemical Geology*, **161**, 59–88.

Ward, P.D., Haggart, J.W., Carter, E.S., Wilbur, D., Tipper, H.W. & Evans, T. 2001. Sudden productivity collapse associated with the Triassic–Jurassic boundary mass extinction. *Science*, **292**, 1148–1151.

Ward, P.D., Garrison, G.H., Williford, K.H., Kring, D.A., Goodwin, D., Beattie, M.J. & McRoberts, C.A. 2007. The organic carbon isotopic and paleontological record across the Triassic–Jurassic boundary at the candidate GSSP section at Ferguson Hill, Muller Canyon, Nevada, USA. *Palaeogeography, Palaeoclimatology, Palaeoecology*, **244**, 281–289.

Waters, R.A. & Lawrence, D. 1987. *Geology of the South Wales Coalfield, Part III, the Country around Cardiff*. Geological Survey of Great Britain—England and Wales—Memoirs: British Geological Survey—BGS Reports. Stationery Office Books, London.

Weedon, G.P. 1986. Hemipelagic shelf sedimentation and climatic cycles: the basal Jurassic (Blue Lias) of South Britain. *Earth and Planetary Science Letters*, **76**, 321–335.

Whittaker, A. 1978. The lithostratigraphical correlation of the uppermost Rhaetic and lowermost Liassic strata of the W. Somerset and Glamorgan areas. *Geological Magazine*, **115**, 63–67.

Whittaker, A. & Green, G.W. 1983. *Geology of the country around Weston-Super-Mare*. Memoirs of the Geological Survey of Great Britain, Sheet 279 with parts of sheets 263 and 295 (England and Wales). HMSO, London.

Wignall, P.B. 2001*a*. Sedimentology of the Triassic–Jurassic boundary beds in Pinhay Bay (Devon, SW England). *Proceedings of the Geologists' Association*, **112**, 349–360.

Wignall, P.B. 2001*b*. Large igneous provinces and mass extinctions. *Earth-Science Reviews*, **53**, 1–33.

Williford, K.H., Ward, P.D., Garrison, G.H. & Buick, R. 2007. An extended organic carbon-isotope record across the Triassic–Jurassic boundary in the Queen Charlotte Islands, British Columbia, Canada. *Palaeogeography, Palaeoclimatology, Palaeoecology*, **244**, 290–296.

Zachos, J., Pagani, M., Sloan, L., Thomas, E. & Billups, K. 2001. Trends, rhythms, and aberrations in global climate 65 Ma to present. *Science*, **292**, 686–693.

Zeebe, R.E. & Wolf-Gladrow, D.A. 2001. *CO_2 in Seawater: Equilibrium, Kinetics, Isotopes*. Elsevier Oceanography Book Series, 65.

Ziegler, P.A. 1990. *Geological Atlas of Western and Central Europe*. Shell Internationale Petroleum Maatschappij B.V., The Hague.

Received 8 January 2008; revised typescript accepted 15 December 2008.
Scientific editing by Ian Jarvis.